Effects of Food Processing Conditions on Local Corrosion of 316L Stainless Steel

Fredrik Waldur
2022

LUND UNIVERSITY

LTH
FACULTY OF ENGINEERING

MASTER THESIS
DIVISION OF PRODUCTION AND MATERIALS ENGINEERING
LUND UNIVERSITY

Supvervisor: Filip Lenrick, Lector
Industrial Supervisor: Martin Adell, Technology Platform Manager
Examiner: Volodymyr Bushlya

Author: Fredrik Waldur
Lund, Sweden, 2022

Avdelningen för Industriell Produktion
Lunds Tekniska Högskola
Lunds Universitet
Box 118
221 00 Lund
Sverige

Division of Production and Materials Engineering
LTH, School of Engineering
Lund University
Box 118
SE-221 00 Lund
Sweden

Printed in Sweden
Media-Tryck
Lund University

Abstract

Pitting corrosion on 316L stainless steel has been widely studied, but knowledge is lacking within food processing environments. A new test setup was developed to enable electrochemical measurements inside a heat exchanger (pasteurizer) where solutions can be heated and cooled rapidly, allowing for corrosion tests of solutions that do not withstand high temperatures for a long period of time. After the development of a new test setup, the effects of chloride, acetic acid and temperature on the pitting corrosion of stainless steel were tested by electrochemical means. The measurements showed chloride concentration has the largest impact on the pitting potential, followed by temperature but the effect trailed off between 80 and 100 °C. The effect of acetic acid was small and difficult to understand, the addition of acetic acid seemed to increase the pitting resistance at low chloride concentrations while decreasing the resistance at higher chloride concentrations. Virtually no difference was seen between the different concentrations of acetic acid used.

Sammanfattning

Gropkorrosion på 316L rosfritt stål har länge studerats, men det finns fortfarande stora kunskapsbrister gällande livemedelsmiljöers påverkan. För att kunna utföra korrosionstester i livsmedelsprocceseringsmiljöer utvecklades en ny testhållare som möjligör korrosionsmätningar inuti en värmeväxlare (pastöriseringsmasking). Då lösningar kan värmas upp och kylas ned snabbt är det möjligt att utföra mätningar i höga temperaturer på lösningar som vanligtvis inte klarar av att befinna sig i höga temperaturer under en längre tid. Efter utvecklingen av den nya testhållaren undersöktes effekten av kloridjoner, ättiksyra och temperature genom elektrokemiska mätningar. Mätningarna visade att kloridjoner har störst påverkan på gropkorrosionen följt av temperaturen där ingen ökad effekt syntes mellan de två högsta temperaturerna (80 och 100 °C). Effekten av ättiksyra var svåranalyserad, vid låga kloridhalter verkade ättiksyran skyddande medan den vid högre kloridhalter minskade skyddet. Ingen skillnad mellan olika koncentrationer av ättiksyra kunde fastställas.

Preface

This thesis was written for Tetra Pak in close collaboration with Production and Materials Engineering at Lund University, Faculty of Engineering. This is the final work for the Engineering Nanoscience programme, with a master's in material science, and is written during the fall semester of 2022. The purpose of this work was to develop our understanding of how food processing environments affect the local corrosion resistance of 316L stainless steel during actual food processing, as compared to a laboratory setting.

I want to give special thanks to both of my supervisors. Filip Lenrick for exceptional supervision and guidance throughout the entire project, and Martin Adell from Tetra Pak for excellent help in the creation of an experimental plan and counselling during data analysis. A big thank you to Volodymyr Bushlya for being my examiner.

Thank you, Klas Holger Jönsson and Mikael Hörndahl for your help with the maintenance and assistance in the development of Sören and the new test holder. I would also like to thank Andrii Hrechuk for his neural network analysis and general help with microscopes. A thank you to Tetra Pak for providing the necessary software and materials for the electrochemical measurements and data analysis, and finally a thank you to Outokumpu for providing 316L stainless steel for the experiments.

Contents

1 Introduction

Stainless steel is a common corrosion-resistant material used for metal parts in both industry and everyday life due to its cost-effectiveness and mechanical properties. The austenitic stainless steel 316L is considered one of the more corrosion-resistant steels, making it suitable for especially harsh environments, such as high chloride-containing solutions or food processing environments. The most important elements in 316L protection against corrosion are chromium and molybdenum, which are mixed into the steel creating a thin protective oxide layer on the surface providing corrosion protection [1]. Stainless steel still suffers from localized corrosion which is one of the most frequent reasons for failure in the industry. Extensive research has already been carried out regarding localized corrosion on stainless steel [2][3][4] but knowledge is lacking in certain areas, such as food processing. The interaction of stainless steel with different environments, such as high chloride concentrations, low pH or high temperatures, can be studied by electrochemical measurements. The reoccurring problem is that commonly used test setups do not mimic real-life processing scenarios where the solution in contact with metal may be under high pressure, high temperature, and high flows.

This thesis is a collaboration between Tetra Pak and Lunds University with the aim of further understanding how the localized corrosion on stainless steel depends on different environmental factors, where the main focus lies on temperature, chloride and acetic acid (HAc)-rich environments. To mimic real-life scenarios, and enable corrosion tests at high temperatures, a test setup for electrochemical measurements inside a pasteurizing machine was developed followed by extensive testing of the different environments.

Disposition of Master Thesis

- A literature study of corrosion mechanisms, measurement techniques and earlier studies.
- Development of test/experimental setup for measurements in pasteurizing machine.
- Sample preparation methodology.
- Electrochemical measurements of corrosion resistance.
- Data analysis of gathered experimental data.
- Conclusions and thoughts about future investigations.

2 Theory

2.1 Stainless Steel

Stainless steel is an iron-based alloy containing a range of different metals depending on grade and type. Stainless steel typically contains between 10 and 30 wt% chromium combined with other metals, such as nickel, titanium, and molybdenum depending on the steel grade. Stainless steels can be divided into four sub-groups depending on their microstructure and composition [5].

- Martensitic - Alloy of chromium and carbon forming a body-centred tetragonal structure (BCT). It is essentially a deformed BCC structure due to the addition of carbon atoms.
- Ferritic - Steel containing chromium with the body-centred cubic (BCC)-structure.
- Austenitic - Face-centred cubic (FCC)-structure obtained by the addition of metals with FCC-structure, such as nickel or manganese.
- Duplex - A combination of austenitic and ferritic (BCC and FCC structure). The amount of each phase depends on the composition of the alloy, usually, it is about 50/50.

316L is an austenitic steel grade, typical compositions are; 17 % Cr, 10 % Ni, 2 % Mo, 0.02 % C [6]. The L stands for "low" due to the low carbon content compared to 316 which could have carbon content 2 or 3 times as high. The high chromium content and the addition of molybdenum make 316L highly corrosion-resistant and one of the most cost-effective steel grades in the market [2]. Since 316L is the material examined in this work, theoretical discussions will largely orbit around chromium and molybdenum and their effects on the passivation layer.

2.2 Passivation of Metal Surfaces

When iron is exposed to oxygen the surface layer reacts, creating a thin layer of FeO_2, a rather unstable oxide. On the other hand, chromium has a thermodynamically stable oxide form, Cr_2O_3, which will replace the unstable iron oxide if the chromium content is above approximately 11 %. This oxide layer is thin, only a few atoms thick (1-10 nm), and is called the passivation layer due to the stabilizing effect it has on the metal [7]. Cr_2O_3 prohibits atoms from reaching the bulk metal where corrosion reactions may happen and thus plays an important role in the protection of stainless steel. It is widely accepted that the passivation layer is in a constant growth/breakdown cycle where the new passivation layer forms from the bulk metal. Tranchida et al. showed that the oxide has a double-layered p-n structure where the outermost layer may react with anions and cations, a behaviour especially important for the film rupture mechanism which will be discussed further in section 2.3 [8]. Adding a few wt% molybdenum increases corrosion protection, especially against pitting corrosion in chloride-rich environments. The mechanisms of the extra protection are still not completely understood, but they showed Mo enters the chromium passivation layer without an increase in passivation thickness. The extra protection is divided into two theories, either Mo mitigates the passivity breakdown or it promotes passive film repair [9]. Since the passivation layer is extremely thin, any perturbations of the film composition, its thickness or the general integrity may create local spots where corrosion is much more likely to happen.

2.3 General Corrosion Mechanism

Corrosion, more specifically wet corrosion is, in simple terms, the attack and breakdown of metals in contact with the surrounding environment. 4 conditions are necessary for corrosion to occur:

1. Cathodic reaction
2. Anodic reaction
3. Electrolyte needs to be present
4. There has to be a connected path between the cathodic and anodic reactions.

A cathodic reaction is a reduction, meaning the oxidation number is decreased and the atom "gains" electrons, you could also think of it as electrons being consumed during the reaction. The reduction of hydrogen ions into hydrogen gas is an example of a typical cathodic reaction.

$$2H^+(l) + 2e^- \rightarrow H_2(g) \tag{1}$$

A reaction that undergoes oxidation is an anodic reaction, electrons are released during the reaction. The loss of metal happens as an anodic reaction.

$$Fe(s) \rightarrow Fe^{2+}(aq) + 2e^- \tag{2}$$

In order for both the anodic and cathodic reactions to arise, an electrolyte needs to be present. A solution is needed for hydrogen ions to form, and iron ions require a solvent to undergo oxidation. By having a pathway for electrons to travel between the anodic and cathodic reaction a galvanic cell is created and the 4 conditions for corrosion are met. A corrosion reaction can be written by combining the anodic and cathodic reactions.

$$Fe(s) + 2H^+(aq) \rightarrow Fe^{2+}(aq) + H_2(g) \tag{3}$$

These two half-cell reactions form a coupled electrochemical reaction, an illustration of the reaction mechanism is shown in figure 1. Metal surfaces are heterogeneous, the poly-crystalline structure creates areas with metal atoms in different energy positions due to the types of defects on the surface, such as grain boundaries, steps, kink sites, vacancies, and ad-atoms [7]. Atoms in high-energy locations, such as the corner of a step or at a grain boundary, are more likely to pass into the solution and therefore corrosion typically initiates from these sites. When uniform corrosion occurs, meaning the entire surface is attacked relatively evenly, the surface is roughly removed layer by layer until it eventually fails. This is caused by the two half-cells "dancing around" the surface leading to an evenly distributed corrosion [10].

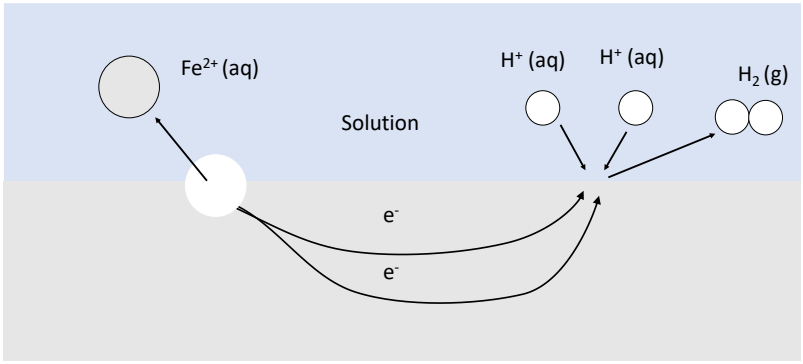

Figure 1: An illustration of the coupled reactions occurring on different sites on the metal surface. Iron is oxidised, leading to the formation of hydrogen gas through a reduction reaction on another location on the surface.

2.4 Localized Corrosion

Compared to the uniform corrosion where the two half-cells move across the surface, localized corrosion has fixed positions of the half-cells leading to corrosion on specific localized spots on the metal surface. There are several different types of localized corrosion, but for the purpose of this work only crevice and pitting corrosion will be discussed. For pitting and crevice corrosion, three distinct stages occurs, nucleation/initiation, metastable growth and stable growth. All three stages will be discussed in the next sections.

2.4.1 Pitting Corrosion Initiation

In pitting corrosion, a local attack confined to a small area of the metal surface breaks down the passivation layer, exposing the metal underneath to the solution. Chloride ions are the most common attacker since it is present in most environments, such as the sea, the human body, food etc. The discussion regarding pitting mechanisms will therefore mainly focus on the effect chloride ions have. The breakdown mechanism for the passivation layer is not yet completely understood but there are three main theories.

1. The penetration mechanism
2. The adsorption mechanism
3. The film rupture mechanism

1. The Penetration Mechanism
Chloride ions are aggressive with a size similar to oxygen atoms (1.81 Å compared to 1.4 Å). The chloride ions penetrate the passivation layer leading to dissolution of the passivation layer at the metal/oxide interface. The mechanism of penetration is not completely known, one theory suggests chloride ions diffuse through the oxide layer through oxygen vacancies due to their similar radius and charge. In the point defect model, it is theorised that the absorption of an anion (eg. Cl^{-1}) into an oxygen vacancy, generates a cationic/oxygen vacancy as a response via a Schottky-pair generation. The new oxygen vacancy may then react with another anion generating yet another cationic/oxygen Schottky-pair and thus the reaction is auto-catalytic. Whether the film breaks down depends on the rate at which cationic vacancies are transported across the barrier while being annihilated by cations released from the metal surface into the oxide film. If the rate of cations released from the metal is lower than the rate at which cationic vacancies diffuse towards the metal surface, the vacancies will condense and form islands between the metal surface and oxide film. As discussed earlier, the passivation layer is in a steady state reaction, constantly growing and dissolving. The condensation of vacancies stops the growth of the oxide film locally on the metal surface which shifts the equilibrium leading to thinning, and eventual breakdown, of the passive film [11]. An illustration of the mechanism can be seen in figure 2.

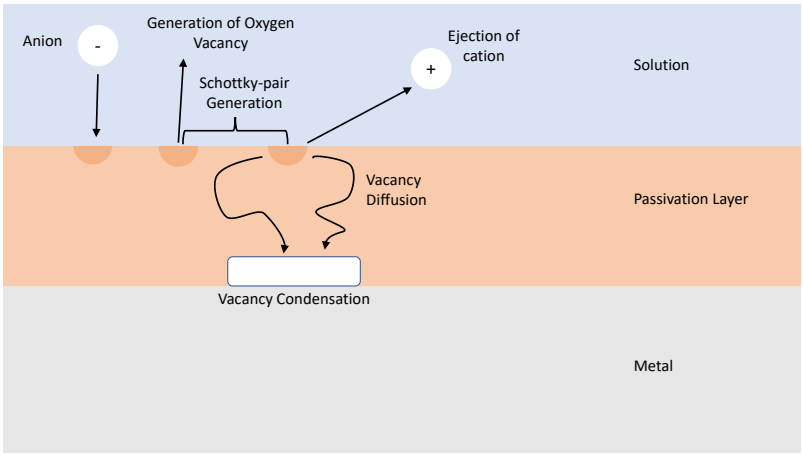

Figure 2: Illustration of a purposed penetration mechanism. An anion absorbs into an oxygen vacancy, the oxide layer responds by creating a Schottky-pair of another oxygen/cationic vacancy. This oxygen vacancy may then react with yet another cation and auto-catalysis has begun. The cationic vacancies may then diffuse towards the metal surface where they condense if the diffusion is not counteracted by the release of cations from the metal surface.

The penetration mechanism has been further studied. B. Zhang et al. found, by using HRTEM and XEDS mapping, that chloride ions are mainly present in the lower part of the passivation layer closest to the metal surface [12]. Their main finding, however, is the suggested diffusion mechanism of chloride ions. The passivation layer is mostly amorphous, but there are small nanocrystals embedded in the film. Along the grain boundaries of these nanocrystals, the diffusion energy is lower for chloride ions compared to the amorphous regions, allowing the diffusion from one oxygen vacancy to the next. If these nanocrystals create a network that reaches from the passivation layer/solution interface down to the metal surface/passivation layer interface (as shown in figure 3), a direct path for chloride diffusion appears which may then locally break down the passivation layer leading to pitting corrosion [12]. Locations, where there is no direct grain-boundary route through the passivation layer, are therefore protected against pitting corrosion, which may explain the randomness as to where pitting initiates.

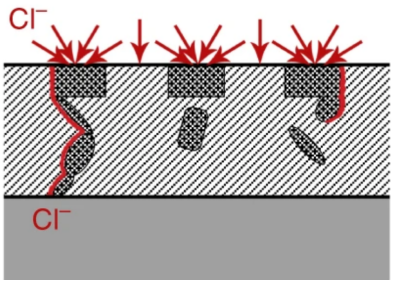

Figure 3: Vacancy diffusion path along the grain-boundaries of nanocrystals in the passivation layer [12].

2. The Adsorption Mechanism

Aggressive ions adsorb into the surface of the oxide film, forming surface complexes that eventually leads to a dissolution of the passive layer. Chloride ions adsorb and forms complexes with metal ions inside the oxide layer, increasing the rate at which they are transferred to the electrolyte. It is the presence of halides that enhances this transportation [13]. The presence of Cr_2O_3 oxide layer for 316L stainless steel has to be discussed in regard to the adsorption mechanism. Chromium exchange with the solvent in presence of chloride ions is extremely slow, thanks to the stabilizing properties of Cr(III) complexes. The low solubility and dissolution (practically non-soluble) for Cr_2O_3 and $CrCl_3$ in water makes the dissolution of the passive layer extremely slow [14]. Therefore, it is unlikely that the breakdown of the passive layer on 316L stainless steel is by the adsorption mechanisms. It is, however, a likely explanation for other types of chromium-free steel.

3. The Film Rupture Mechanism

In this proposed mechanism, chloride ions penetrate through flaws or cracks in the oxide film. The chloride ions further develop the pre-existing flaws through hydration or dehydration events inside the film, which expands it. Hoar assumed this was a form of mechanical stress that eventually broke the passive film [15]. Sato, on the other hand, postulates another theory of how the film ruptures due to electrostatic pressures. When the film becomes thick enough the electrostatic pressure creates mechanical stress on the film that ruptures the passive layer [16]. The electrostatic forces inside the passive layer are due to the pn-junction behaviour [17].

From this small literature review, it is evident that a lot of research regarding the mechanisms for passive layer breakdown has been done. The mechanism is complicated and there is still no generally accepted theory. For 316 stainless steel, another possible pitting initiation exists. It is common to add small amounts of manganese to stainless steel, especially 316L. Manganese can be added as a substitute for nickel which leads to improved machinability. However, manganese forms micron-sized manganese-sulfide (MnS) inclusions in the passivation layer. These inclusions act as sites for pitting initiation, and removal of MnS inclusions leads to increased corrosion resistance [18].

2.4.2 Crevice Corrosion Initiation

Crevice corrosion is localized corrosion underneath geometrical clearances, such as under bolt heads, under gaskets or seals, or under other corrosion products stuck on the surface. There are two main stages of crevice corrosion, initiation and propagation. Fontana and Greene proposed the mechanism for initiation shown in formula 4 and 5 [19]. Across the entire surface, including at the crevice, oxygen reduction occurs, as well as the dissolution of metal (M).

$$M \longrightarrow M^+ + e^- \tag{4}$$

$$O_2 + 2H_2O + 2e^- \longrightarrow 4OH^- \tag{5}$$

The metal freely exposed to the solution has a steady flow of oxygen toward the surface. Due to the limited amount of diffusion at the crevice, oxygen will begin to deplete, and the concentration of metal ions will increase. This leads to a concentration gradient between the crevice and the bulk surface, furthermore, the concentration of positively charged metal ions increases in the crevice. This positive charge increase is balanced by the migration of other, negatively charged ions, such as Cl^-. Chloride ions are known to break down the passivation layer, and so the crevice corrosion initiates.

2.4.3 Metastable Pits

So far, we have seen that pit initiation happens due to the breakdown of the passive film. The breakdown is aided by the presence of chloride ions which locally disturbs the oxide layer, but what happens immediately after the oxide layer breaks down? The bulk metal is then exposed to the electrolyte allowing the corrosion reaction to take place. A cover layer is formed over the newly created pit by remnants of the oxide layer or from corrosion products formed at the same time. This cover layer may prevent the dissolution of the metal beneath, allowing time for repassivation of the protective oxide layer. This initial corrosion stage is called metastable pitting and is an intermediate stage before the transition to a stable pit growth or the repassivation of the passive layer. The repassivation can only happen if the metal is below the critical pit stability level [20]. A high chloride concentration may easily perforate this cover layer and thus metastable pitting may be less prominent in chloride-rich environments.

2.5 Pourbaix Diagram

A Pourbaix diagram is a predominance diagram calculated from the pH and standard reduction potential of the system, and describes possible thermodynamically stable phases for different systems. Using a combination of thermodynamically measured data and the Nernst equation (equation 6), stable phases can be plotted as different regions, where each region represents the most predominant component for a system in equilibrium [21]. The Nernst equation allows calculations of the redox potentials of a reaction. The redox potential is a measurement describing how easily a system accepts electrons which in turn shows the system's overall reducing or oxidizing capabilities. In the Nernst equation, R is the gas constant, T temperature in Kelvin, n is the number of electrons transferred in the cell reaction, F is Faraday's constant and Q the reaction quotient, E^0 the standard reduction potential and E is the resulting cell potential.

$$E = E^0 + \frac{RT}{nF} lnQ \tag{6}$$

A Pourbaix diagram of pure Iron, figure 4 was derived using KTH's programme Medusa and Hydra [22], (cr) indicates a crystalline state and E_{SHE} is the potential of the solution according to the Standard Hydrogen Electrode (SHE). Horizontal lines show that pH has no effect on the reaction, for example the oxidation of Fe(cr) into Fe^{2+}, since no hydrogen atoms are

present in that reaction $Fe \rightleftharpoons Fe^{2+} + 2\,e^-$. Vertical lines show the equilibrium is potential-independent since no electrons are present in the reaction. The green dotted lines indicate the stability of water inside the system, thus above the green lines water will split into oxygen and hydrogen. If the stable phase is the metal, in this diagram pure Fe, then we say the system is immune, and corrosion cannot happen. For pure Fe at pH 7 without an applied voltage, the metal is outside the stable phase and thus corrosion will occur forming $Fe(OH)_2$, what is usually refered to as red rust. The Pourbaix diagram also tells us if an oxide layer will form on the surface of the metal. For Fe, $Fe(OH)_2$ will form around pH 9-13 which creates a protective layer against corrosion. To remove metals from corrosion phases in the diagram there are three possible ways.

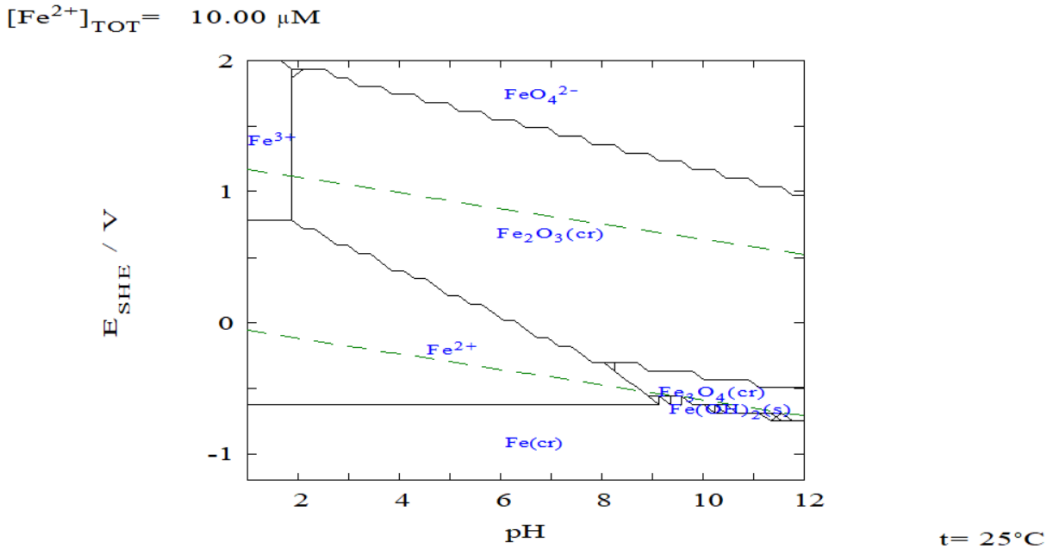

Figure 4: A Pourbaix diagram of pure iron at room temperature where each region shows a stable iron phase. E_{SHE} is the potential of the solution. The two phases on the bottom right are Fe_3O_4 and $Fe(OH)_2$.

A Pourbaix diagram for Cr_2O_3 is useful to further understand why a passivation layer of Cr_2O_3 provides better corrosion resistance (figure 5) compared to pure iron. Comparing the area of the stable Cr_2O_3 phase with the stable phase of $Fe(OH)_2$ in figure 4, Cr_2O_3 clearly has a larger stable region which is why the Cr_2O_3 passivation layer is a good corrosion inhibitor.

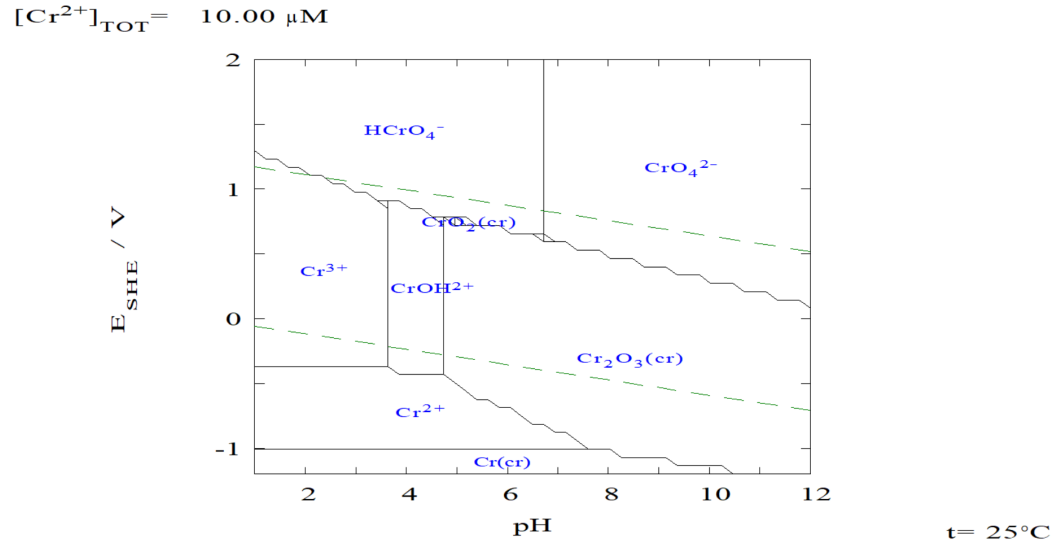

Figure 5: Pourbaix diagram for Cr_2O_3

In an electrochemical system, if a metal is outside the immunity region, there are possible ways to force it into a stable, immune,

region.

1. Lower the electrode potential into the stable Fe-phase.
2. Increase the electrode potential into a phase where a protective oxide layer forms.
3. Increase or decrease pH so that the protective oxide layer forms.

Pourbaix diagrams use, as already stated, the potential vs pH. This means all other parameters have to be kept constant, such as pressure, ion concentration, and temperature. One could instead change the pH axis and plot potential vs $[Cl^{-1}]$ to see how the Chloride concentration affects the different regions. This may be especially useful to do in order to compare diagrams calculated in software with actual measurements to see if the areas match the experimental measurements. Another thing to note is that the Pourbaix diagram does not take kinetics into account, thus a non-stable phase may never react due to the lack of driving forces.

2.6 Electrochemical Measurements

Electrochemical measurements are a relatively quick way to analyse the corrosion resistance of a metal, as compared to leaving the metal in a solution and wait until corrosion happens, a process that may take years. Applying a voltage to a metal sample forces it into unstable regions where the passive layer breaks down. Therefore, electrochemical measurements are well suited for laboratory work where time is of the essence. A classical three-electrode cell uses a reference electrode (RE, (3)), a counter electrode (CE, (2)) and a working electrode (WE,(1)), see figure 6. The current is measured between the working and counter electrode, and the reference electrode determines the solution potential. The RE has to be placed as close to the WE as possible, otherwise, there will be a significant potential drop between the WE and the RE due to resistance in the solution, especially if the ion concentration is low [23]. The majority of the current passes between CE and WE. While the passive layer is intact, the current is low but as it breaks down a rapid increase in current will be seen since electrons and ions may freely flow between the WE and CE. So a rapid increase in current indicates the formation of a pit.

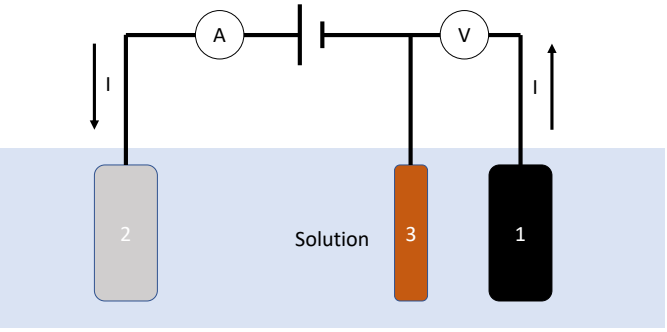

Figure 6: A classical three-point system for electrochemical measurements. (1) is the working electrode connected to the sample, (2) is the counter electrode and (3) is the reference electrode.

2.6.1 Linear Potentiodynamic Polarization

A useful electrochemical measurement is the linear potentiodynamic polarization measurement where the voltage is linearly increased while the current is carefully monitored. As the passive layer breaks down, the bulk metal is exposed to the surface and there will be a sharp increase in the measured current due to the generation of electrons during the oxidation of iron. The potential at which this happens is called the pitting potential, or E_{pit}, and gives a value which could be compared when running experiments on different environments or metals. A lower E_{pit} indicates worse corrosion resistance. Even if E_{pit} is a good value to compare metals and environments towards each other, it is difficult to translate the values into what the corrosion resistance is in the physical world. Furthermore, it is not possible to see the location of the pits, or the quantity of them. Only that we had a breakdown of the passive layer, the electrochemical measurements provides limited descriptions of how the breakdown actually happens.

2.6.2 Open Circuit Potential

The Open Circuit Potential (OCP) is the measured potential between the WE and the environment where the RE determines the resting potential of the solution with no applied voltage. The OCP is the maximum potential difference between the WE and RE since there is no current flowing. At the OCP, the system as a whole is at equilibrium, it is sometimes referred to as the corrosion potential, since metals will corrode at OCP, given enough time [24]. The OCP of systems is often measured for 10 minutes up to a couple of hours before initiating the linear potentiodynamic polarization to let the system stabilize.

2.6.3 Oxygen Evolution and Transpassive Breakdown

When the applied voltage reaches high levels during electrochemical measurements it may affect both the solution and metal in non-desirable ways. At high potentials, water is split into oxygen and hydrogen. Looking at the pourbaix-diagram shown in figure 5, the stability region for water is shown as green dotted lines. Above the top line oxygen evolution occurs:

$$2H_2O(l) \longrightarrow O_2(g) + 4H^+(g) + 4e^- \tag{7}$$

This means, at high potentials, an increase in current could just be the extra electrons created by the dissolution of water.
The transpassive breakdown occurs when a high positive potential is applied to the metal, forcing it into an unstable region. The passivation layer is then dissolved, exposing the metal to the solution, very similar to the passive film breakdown and local corrosion mechanisms described in section 2.3 [24]. Therefore, careful evaluation of the obtained polarization curves is important when the applied voltages reach high levels (around 1V and higher with respect to the SHE electrode).

2.7 Pasteurizer

A pasteurizer is a type of heat exchanger used to quickly heat liquids followed by rapid cooling. This makes it possible to heat treat solutions that cannot withstand heat for longer periods, like milk. When milk is exposed to high temperatures, the proteins denature destroying the milk in the process. Therefore, it has to be quickly cooled after reaching temperatures above the denaturation temperature. The pasteurizing process is required to increase the shelf life of products by killing germs and special enzymes that would otherwise deteriorate the products too quickly. Figure 7 provides a schematic of the basic principle of a pasteurizer as well as an image of the actual pasteurized used for experiments in this thesis. The solution is poured into the feed tank and pumped through heating pipes followed by the test holder where corrosion experiments are done. Thereafter it is pumped through a series of cooling pipes before it is pumped back into the feed tank, repeating the cycle.

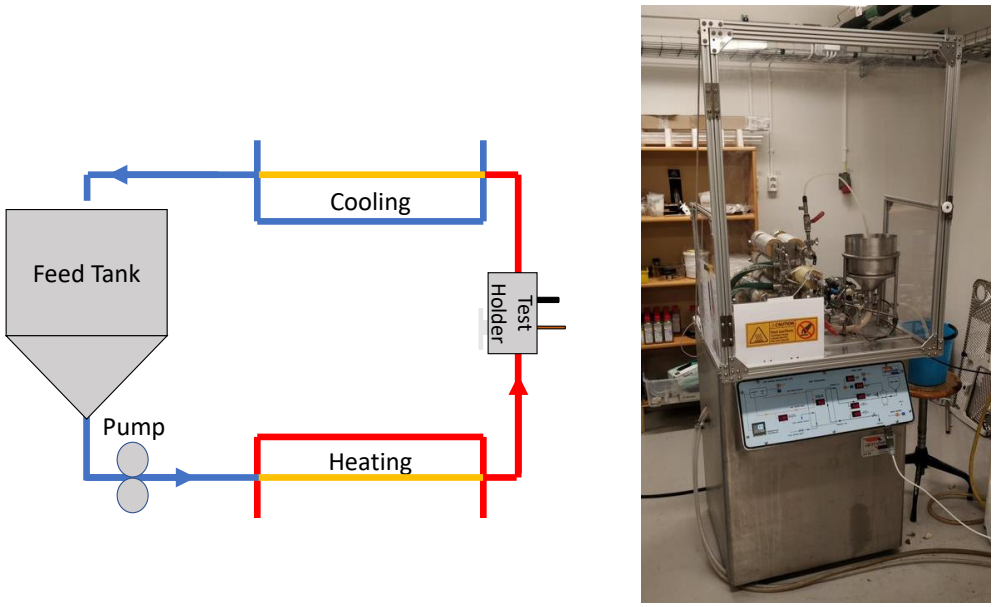

Figure 7: Schematic of the basic principle of a pasteurized along with an image of the Armfield pasteurizer used in this thesis.

3 Development of Test Method

3.1 Test Holder Development

The development of a test holder, making it possible to do electrochemical measurements inside the pasteurizer, was a key part of this thesis. Test holder prototypes were designed in Solidworks and 3D-printed with polylactic plastic (PLA). The first

designs had both the RE and CE at an angle, a design that made it difficult to insert the reference electrode in close proximity to the metal sample. Therefore, after a redesign, the test holder illustrated in figure 8 was produced. The reference electrode should be in close proximity to the sample, no more than a couple of millimetres away, as illustrated by figure 8 (a), figure 8 (b) is an image of the test holder during an experiment with RE, CE and WE marked. The 3D printed prototype did not work as an actual test holder due to the low (≈55°C) glass transition temperature (T_g) of PLA meaning it starts deforming at temperatures below the intended test environments [25]. Therefore, Polyoxymethylene (POM) plastic was used instead, mainly because it was readily available in-house and is easy to work with. After running some experiments at 60°C the test holder started deforming, rendering it useless, and a new holder had to be created. Before choosing a new material, a small specification list was made to ensure all the new materials had all required properties fulfilled.

- Handle temperatures up to 150°C without deforming under pressure.
- Inert material that does not chemically react with intended environments, such as high chloride concentrations, acetic acid (low pH), and milk.
- The material must be an insulator, if it is conductive electrochemical experiments are impossible.

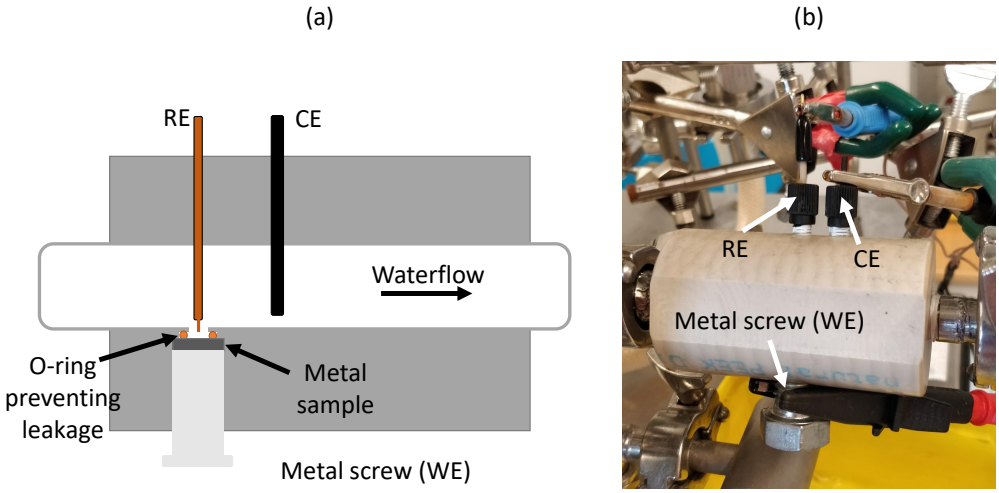

Figure 8: An illustration of the test setup (a) with electrodes, metal sample and O-ring marked. The actual PEEK-plastic test setup in the pasteurizer during the experiment (b) with electrodes connected to the potentiostat with ordinary crocodile clamps.

Polyether ether ketone (PEEK) plastic was chosen as the new test holder material. It has a T_g of 150°C, high chemical resistance and it is an insulator [26]. TECAPEEK MT natural was the actual name of the specific PEEK-type used to create the test holder shown in figure 8 (b).

Generally, the design of the test setup aimed to allow for pitting corrosion but no other types of corrosion. The standardized method used for these types of tests is the Avesta cell, which looks similar to our design but it has a filter paper instead of an O-ring connected to a water inlet allowing for constant flooding of distilled water which eliminates crevice corrosion between the O-ring and the metal sample [27]. The problem with having an external system of distilled water constantly flooding the filter paper is the pressure. Since experiments up to 140°C are planned, the solution has to be pressurized. For example, the vapour pressure for water at 140°C is about 4 bar, which means an overpressure of 4 bar has to be applied to keep water in liquid form. This overpressure has to be matched by the flooding of distilled water which is not trivial to do. The pasteurizer will provide a constant flow of solution through the test holder which decreases the amount of stagnant solution that may lead to crevice corrosion underneath the O-ring. Therefore, the simpler design with only an O-ring was deemed good enough. This design has been used for all the experiments in this thesis

As will be discussed in the Results, part of the uncertainty and large error margins may be due to pitting initiation in close proximity to the O-ring or crevice corrosion underneath the O-ring. For this reason, a new prototype for furture experiments was developed that may increase the amount of pitting corrosion. The metal samples are moulded into an epoxy puck with some type of conductor attached to the backside of the sample, in the prototype shown in figure 9, the aluminium tape was used as a connector. This way, the O-ring never touches the sample removing the possibility of crevice corrosion. The new holder has not yet been tested but it looks promising. The main risk is in the interface between metal and epoxy, where corrosion may prefer initiated. This new holder design has not been tested and was not used for any of the experiments in this thesis.

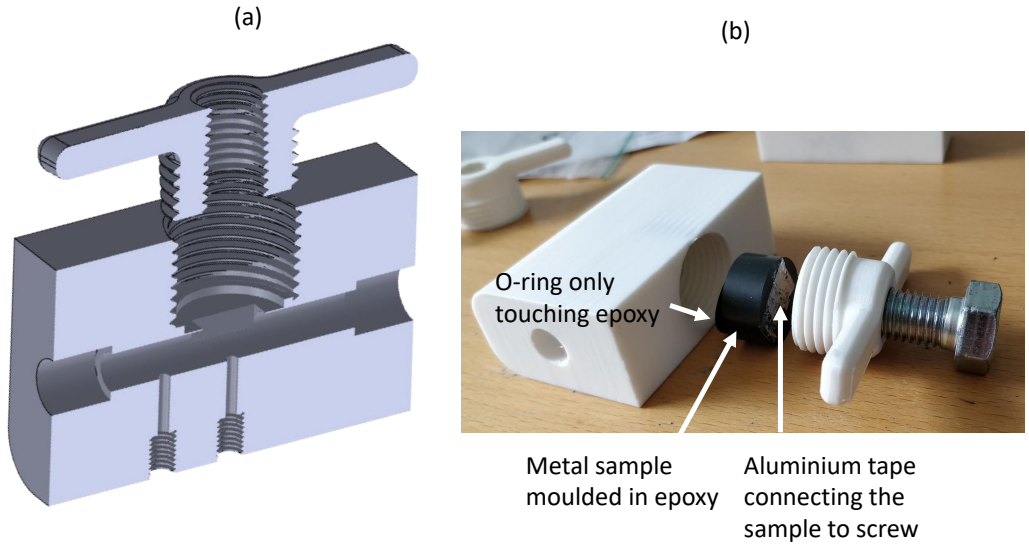

Figure 9: Model of a new test holder. (a) is the CAD drawing and (b) is the 3D-printed model showcasing the O-ring, the sample moulded inside epoxy with aluminium tape attached to it and the metal screw connecting the sample.

3.2 Problems During Development

Several problems arose during the development process. To avoid crevice corrosion several different methods were tried to protect the area underneath the O-ring. Nail-polish was too soft even after drying for 24 hours, car polish remained intact during the entire test but the corrosion began at the interface between the polish and metal. Therefore the most reliable result came from doing nothing to the samples since the exposed area would be the same for each measurement. With car polish, the exposed area and geometry of the polish varied between tests. Another problem during early experiments was a high background current that seemed to appear randomly. Usually, the background current was in the order of 0.1 - 0.01 μA but suddenly the background current could be as high as 10 μA. Some time was therefore spent troubleshooting, ruling out possible errors one by one. The following things were tried;

- Changing RE, CE and WE one by one, ruling out any errors.
- The Nova Autolab was re-calibrated.
- The metal screw was changed.
- Experiments were run inside a cup instead of the test holder.
- The pasteurizer was separately connected to ground.
- Tests were run with the pasteurizer turned off.

- All large machines in the workshop were turned off/on.

The problem with background current arouse when the pasteurizer was turned on, but not always which was quite perplexing. It was noted that the background current was present mainly during working hours. It was concluded that the background current probably came from large fans used during renovations of the buildings, when the builders were finished with the renovation the background current disappeared.

Large deviations in pitting potential were found during early measurements, the reason was precipitated NaCl on the O-rings. The O-rings were reused but not washed properly in the beginning since it was not enough to just rinse them. Some images and more comments about this small analysis are found in the appendix A.6. With the right technique, the O-rings could be properly cleaned and reused without any effects on the measurements.

The Ag/AgCl RE is specified for temperatures up to 90 °C which could potentially become a problem in the future. After speaking to the manufacturer, 100 °C was no problem, but at higher temperatures the risk of destroying the RE increases. Running tests at 100 °C showed no effect on the RE, but higher temperatures might. However, the manufacturer suggested running tests at higher temperatures and reporting back to them if the RE failed, if it failed they would send a new one. If the electrode cannot handle temperatures that high, a new solution is necessary.

3.3 Pasteurizer

The pasteurizer was fitted with protective barriers for potential hot water/steam leakage. A pressure valve of 6bar was also installed which should allow for temperatures around 150°C. A safety protocol and risk analysis was created and can be read in appendix A.3.

4 Experimental Method

4.1 Experimental Setup and Procedure

4.1.1 Material

The material used in this study was mainly 316L (Supra 316L/4404) from Outokumpu, the actual chemical composition of this steel is given in table 1. About the first 1/3 of the experiments used a different set of 316L because the material from Outokumpu had not yet arrived. This early batch of 316L matched the experiments with Outokumpu's 316L.

Table 1: The actual chemical composition of 4404 316L stainless steel.

Chemical Composition (wt%)								
C	**Si**	**Mn**	**P**	**S**	**Cr**	**Ni**	**Mo**	**N**
0.017	0.60	0.96	0.032	0.001	17.1	10.2	2.04	0.037

4.1.2 Potentiodynamic Polarization Measurements

The samples were prepared by using a puncher (12mm) on a 1.5 mm thick 316L metal sheet. The samples were ground by hand in steps with SiC (220, 500 grit) grinding paper finished by MD-Piano 1200. Thereafter, samples were left to oxidize for at least two weeks in the open air. Before inserting samples into the pasteurizer, they were cleaned with distilled water followed by ethanol and then blow-dried with air. The samples were then inserted into the holder which was placed inside the pasteurizer (Armfield FT74), the exposed area was 0.385 cm^2 (O-ring inner diameter was 0.7 cm). The solution was prepared with cold tap water, regular table salt without iodine and acetic acid from Perstorp (24%). The solution was heated inside the pasteurizer until the proper temperature was reached before measurements began, the temperatures varied from the set value $\pm$ 2°C. The water flow inside the pasteurizer was 8.2 ml/s (achieved by a pump frequency of 14.3 Hz). Electrochemical measurements were done by using a conventional three-point electrode test setup with the potentiostat Autolab PGSTAT101 and the software Nova (2.1.3). An Ag/AgCl reference electrode was used together with a glassy carbon counter electrode. OCP measurements were done for 30 minutes. The linear polarization scan rate was 0.166 mV/s. The pH was measured for each solution after the

initial 30 minutes of OCP. Calibration of pH and redox electrodes was done weekly, and the reference electrode was checked once every month. The starting potential was set to the measured OCP value and the stopping potential was set to either 1.5 V (Ag/AgCl) or if the current exceeded 500 μA/cm^2. The pitting potential was defined as the value when a stable current exceeds 10 μA/cm^2. The test procedure largely follows the Swedish standard SS-ISO 15158:2014 [28]. Deviation from the procedure are not using the Avesta cell and not using reagent-grade chemicals and high purity water, since food processing conditions are to be mimicked. Furthermore, if pitting was initiated above 1.2V (Ag/AgCl), it was not deemed pitting corrosion but a result of transpassive breakdown. After the corrosion test was done, the samples were cleaned with distilled water and inspected with an optical microscope. Data analysis was carried out in Excel, Minitab and Matlab.

The Ag/AgCl reference electrode potential was converted into the SHE potential by using standard tables, generally, at the potentials used in this thesis $E_{SHE} = E_{Ag/AgCl} + 0.197V$. The Ag/AgCl compared to the SCE electrode is about -0.014V [29].

A standard potentiodynamic polarization measurement is plotted in figure 10. The sharp increase in current at the beginning of the measurement is explained by the starting potential (OCP) where the current typically is 0. Since the current is plotted logarithmically, there seems to be a sharp increase at the very beginning. At a certain potential, the current increases 10-fold and if the current is stable above 10 μA/cm^2, this is the pitting potential E_{pit}.

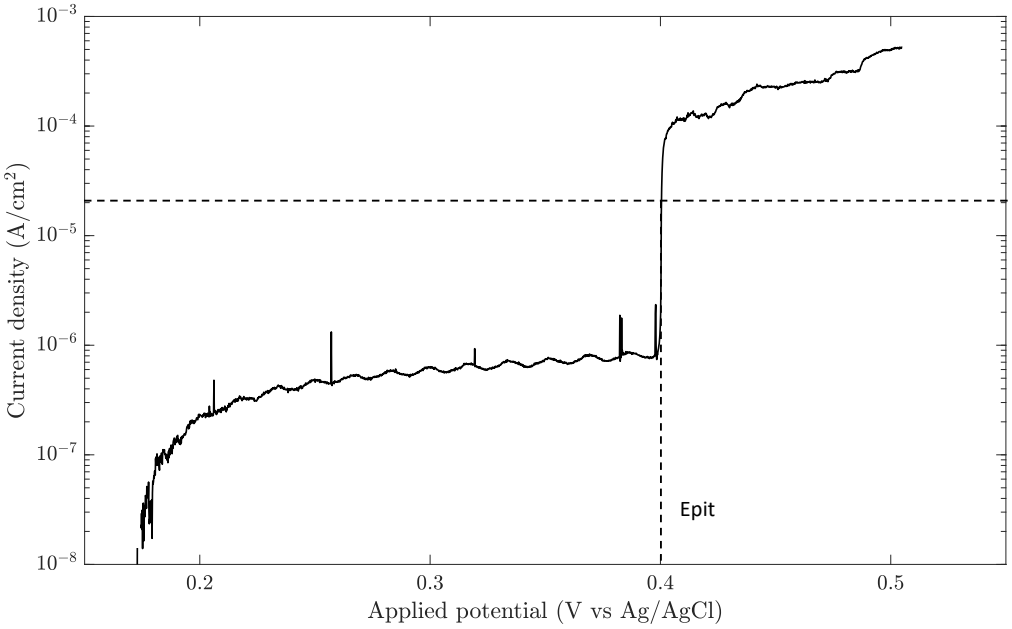

Figure 10: A typical potentiodynamic polarization curve where the sharp increase in current corresponds to pitting initiation. The vertical corresponds to the determining current for pitting initiation (10 μA/cm^2).

Table 2: Average measured pH values for different temperatures at different acetic acid concentrations (0-3 %).

	Concentration Acetic Acid (%)		
Temp (C)	**0**	**1**	**3**
30	8.19	2.73	2.45
45	8.51	3.04	2.48
60	8.23	2.76	2.43
80	7.10	2.80	2.39
100	6.75	2.78	2.40

5 Result & Discussion

The basis for the data analysis is a total of 207 electrochemical measurements. The average measured pH values for the different environments are provided in table 2. Increasing temperature leads to a decrease in pH at 0% acetic acid, an expected behaviour. Looking at the equilibrium formula for pure water; $H_2O \rightleftarrows H^+ + OH^-$, increasing temperature moves the equilibrium to the right, increasing the number of hydrogen ions in the solution and thus decreasing pH. The solution is still neutral though, since pH = pOH.

Most of the pits formed at the edge of the O-ring, and thus the question of whether we are measuring pitting corrosion or crevice corrosion must be discussed. Crevice corrosion tends to have a slower development due to the stagnation of the solution within the crevice, leading to a gradual increase of ions. This also leads to a more gradual increase in the measured current. However, in most of the measurements (except for at low chloride concentrations, as will be shown in the next section), the increase in current was very abrupt which signals we do actually see the formation of pits. Furthermore, there is a continuous flow of water which limits the formation of stagnant solution and thus the risk of crevice corrosion is decreased. Therefore, it will be assumed what we measured is pitting corrosion, even though the formation of the pits generally occurred at the very edge of the O-ring.

5.1 Low Chloride Concentrations and Transpassive Breakdown

At low chloride concentrations, pitting was not always the main mechanism of breakdown. A slow but steady increase in current suggests crevice corrosion due to the linear evolution of the passive film breakdown. For example, in figure 11), three different measurements run at 30°C, 10 ppm NaCl and 0% HAc is plotted, all of which have a gradual increase in current. As described in section 2.6.1, pitting is characterized by a sharp increase in current, the opposite is seen in this figure. This typically indicates either crevice corrosion or a transpassive breakdown of the thin film [30][2]. The current start to increase at about 0.9V (Ag/AgCl electrode) which corresponds to about 1.1V vs SHE electrode. At 1.1V vs SHE, the chromium oxide is far from the stable state according to the pourbaix diagram, (figure 5), indicating transpassive breakdown. Another possible explanation for the gradual current increase is the oxygen evolution where water is split into oxygen and hydrogen ions, generating electrons in the process (see reaction formula 7). Since the increase in current is not from pitting, these results will be excluded from all pitting results presented.

Further analysis of where the transpassive breakdown begins is needed, otherwise "false" pitting potentials may be added. For example, figure 12 presents four different measurements at 45 °C, 10 ppm NaCl and 0% HAc. Both curve a and d seem to have a sharp increase in current at about 1.05 and 0.95 V vs Ag/AgCl, this is about the region where the chromium oxide becomes unstable. It is also known, as discussed earlier (2.6.3), that the transpassive breakdown is very similar to the pitting initiation. Therefore, these sharp increases in current that certainly looks like pitting initiation, may not be actual pits. Earlier studies have used different values for where transpassive breakdown in linear polarization measurements occurs, the values range from 1-1.2 V vs Ag/AgCl [2][31]. If the pitting initiation is above 1.2V, it will be discarded and assumed to be from the transpassive breakdown.

Analysis of the potentiodynamic curve to determine the pitting potential is not always as clear as in the example shown earlier (figure 10). Figure 13 shows a measurement done at 100°C, 10 ppm and 3% HAc. α points towards a bump in current which is present in all measurements at 100°C at low chloride concentrations. What causes this bump is not perfectly clear, it may

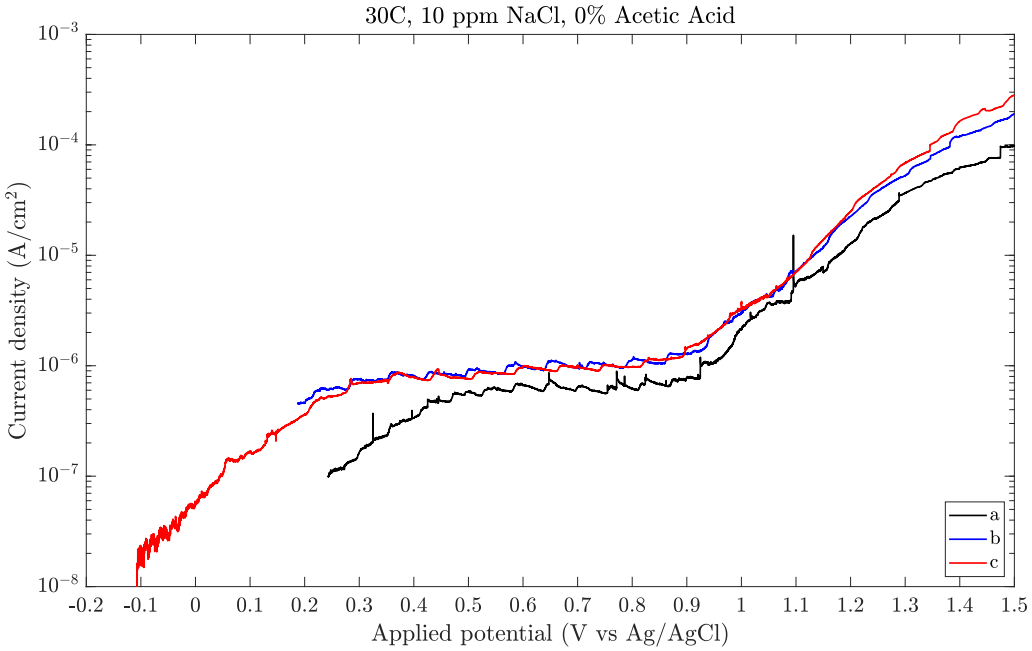

Figure 11: Examples of a linear polarization where pitting corrosion did not occur. a, b and c are three different measurements at 30 °C, 0% HAc and 10 ppm NaCl, all of them show a gradual current increase.

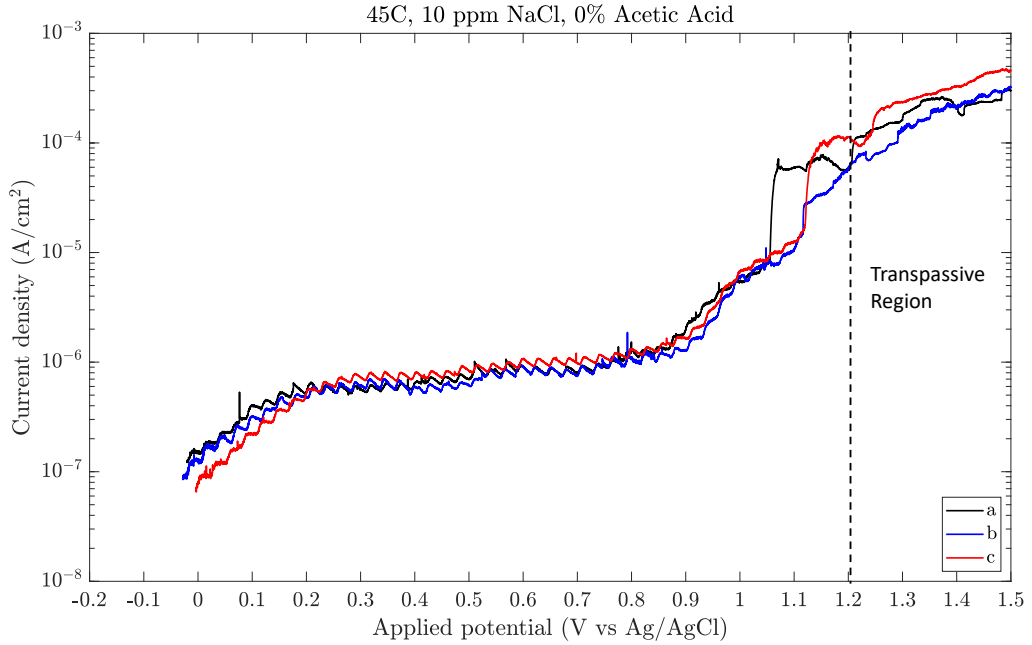

Figure 12: A potentiodynamic measurement where the transpassive region is marked.

be due to the dissolution of MnS inclusions as reported in a study by J.O. Park et al [32]. The definition used for pitting potential is when the current density reaches 10 μA/cm^2, however that value may not be applicable for all cases. At high temperatures, the heating unit in the pasteurizer requires a considerable amount of power which the potentiostat picks up. The oscillating behaviour of the curves is the heating unit being turned on and off. Because the current exceeds 10 μA/cm^2 due

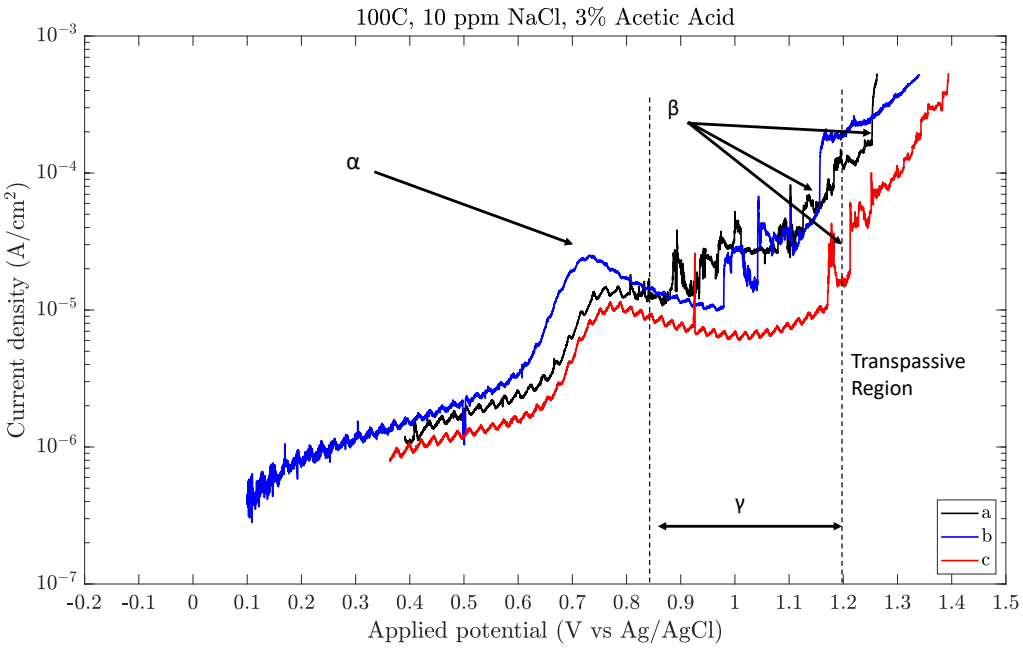

Figure 13: Three measurements in the same environment where the results are difficult to interpret. α points towards a "bump" in current, β towards what could potentially be defined as the stable pit formation γ displays an area where metastable pitting seems to occur.

to the bump in the current before any pitting behaviour initiates, more hands-on analysis of the pitting potential is required. A pit is characterized by a sharp increase in current, followed by a high, stable current. The area marked by γ has both rapid increases followed by decreases in current, thus these are not considered pitting potentials. A decrease in current after a rapid increase indicates a metastable pit, as discussed in section 2.4.3. The pitting potential for these measurements could therefore not be determined, however, if pitting potentials were to be extracted from these measurements β points towards increases in current followed by a large stable current. These areas are either in close proximity (curve (b)) or above the transpassive region (curve (c) and (a)) and were therefore not counted as pitting potentials.

5.2 Chloride, Acetic Acid and Temperature

Figure 14 compares two experiments run at the same temperature and acetic acid concentrations but with two different chloride concentrations, 10 000 ppm (black) and 100 000 ppm (orange). The 10 000 ppm curve shows clear signs of metastable pitting, with sharp current increases without stable pit formation before the actual pit forms. At higher chloride concentrations (100 000 ppm) virtually no metastable pitting has been observed for any experiment. This behaviour, that lower chloride concentrations give more metastable pitting, has been observed throughout the experimental process. As earlier discussed, looking at figure 13, there is basically only metastable pitting until the transpassive region is reached for low chloride concentrations. A possible explanation for this behaviour is that higher chloride concentrations easier perforate the cover layer created during the metastable phase, as discussed in 2.4.3. Therefore, corrosion goes from a stable passivation layer to a stable pitting immediately [20].

Temperature and acetic acid effect on the pitting potential are plotted in figure 15 with regions without pitting initiations for some temperatures marked as a dotted area. A higher chloride concentration has a large impact on the pitting potential since all combination of temperature and acetic acid leads to a decrease in pitting potential as the chloride concentration increases. This behaviour is well documented and follows earlier studies regarding chloride effects on pitting potentials [2][3][4]. The 0% acetic acid plot shows that increasing temperature decreases the pitting potential, up to 80 °C. At higher temperatures, there is a further decrease in pitting potential, but 100°C does not decrease the pitting potential compared to 80 °C. The same pattern can be found for both 1% and 3% acetic acid, 80 and 100 °C generally have the lowest pitting potential but there is

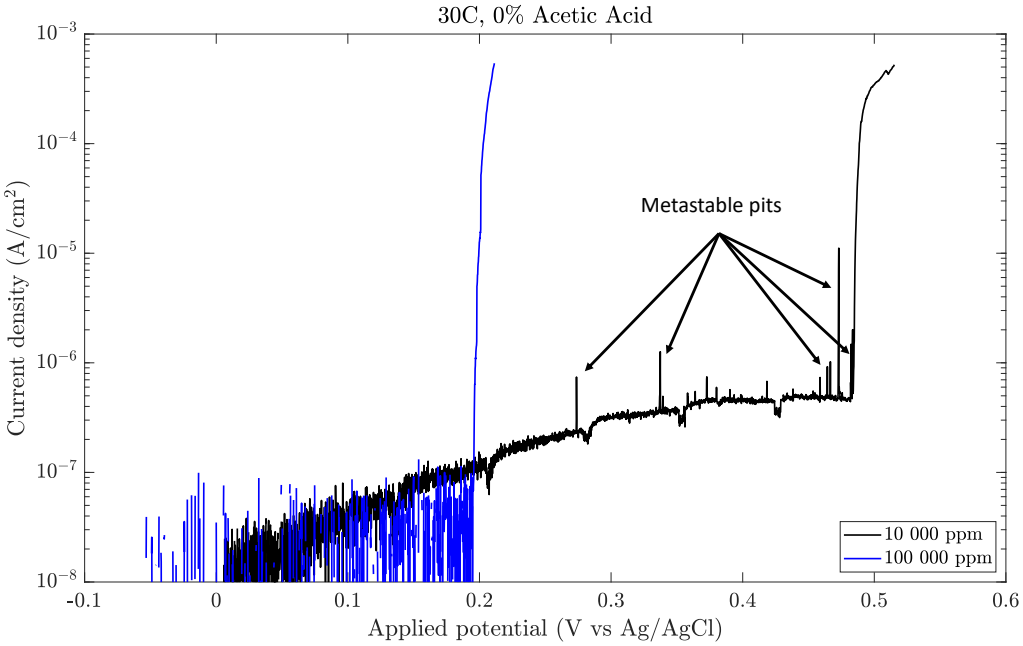

Figure 14: Comparison of two different NaCl concentrations run at 30 °C and 0% acetic acid. Lower chloride concentrations generally lead to more metastable pitting as indicated by the arrows.

virtually no difference between the two whereas for 30, 45 and 60 °C, the pitting potential decreases for each temperature step. For 0%, no pitting was observed at 10 ppm for 30, 45 and 60 °C. For 1% no pitting at 10 ppm was observed for 30 °C and finally for 3% acetic acid pitting was only observed for 60 °C, although only 1 out of 3 measurements had pitting while the other two measurements did not show pitting. Looking at pit formation at 10 ppm NaCl, adding 1% acetic acid increased the pit formation since both 60 and 45 °C showed pitting. This indicates acetic acid decreases the corrosion resistance, however, when 3% acetic acid was added only 60 °C showed pitting behaviour meaning a higher concentration of acetic acid does not seem to further decrease the pitting potential.

To further analyze the impact of acetic acid on pitting potential, the pitting potential was plotted at different temperatures where each line represents one acetic acid concentration, as shown in figure 16. Generally the pitting potential for 0% acetic acid at 100 000 ppm NaCl is higher than for 1% and 3% acetic acid, with the exception for 100 °C where the pitting potential is within the standard deviations. The absence of pitting potentials at low chloride concentrations can be seen in this graph as well. Apart from what has already been discussed, acetic acid does not seem to have a large impact on the pitting potential, a result that is quite surprising. The chromium pourbaix diagram in figure 5 suggests a breakdown of the stable film at about pH 4, although this pourbaix diagram does not take the complex composition of 316L into account. The addition of molybdenum may change the chemistry enough to withstand the decrease in pH. Why 1% acetic acid promotes pitting at 10 ppm while 3% inhibits is not completely clear. A possible explanation may be the adsorption of acetic acid on the steel surface. A positive charge is applied to the metal sample while HAc loses its hydrogen ion, becoming the polar Ac^- which then may adsorb on the sample surface, perhaps guided by the positive applied potential. This layer of adsorbed acetic acid might deflect chloride ions, protecting the surface. The concentration when 1% acetic acid is added might be too low to create a protective barrier while 3% is high enough to deflect the reactive chloride ions. When the concentration of chloride ions increases, this protective barrier is not enough to protect the surface and therefore the effects of low pH take over which could explain why the pitting potential is lower for 100 000 ppm when acetic acid is present compared to without. Acetic acid has been reported to act as a protective barrier in earlier studies [33] where it decreased the number of pits, but the size of the formed pits was enlarged. A thorough analysis of acetic acid effects on pitting corrosion by Amri et al. found that acetic acid does not participate in the H_2 evolution (reaction formula 1), meaning it does not actively take part in the corrosion mechanism. They found acetic acid acted as a proton-buffer at the cathode which should lead to increased susceptibility of corrosion - but could not find such correlation during polarization measurements [34]. The effect of acetic acid on pitting corrosion, and the mechanism, is not

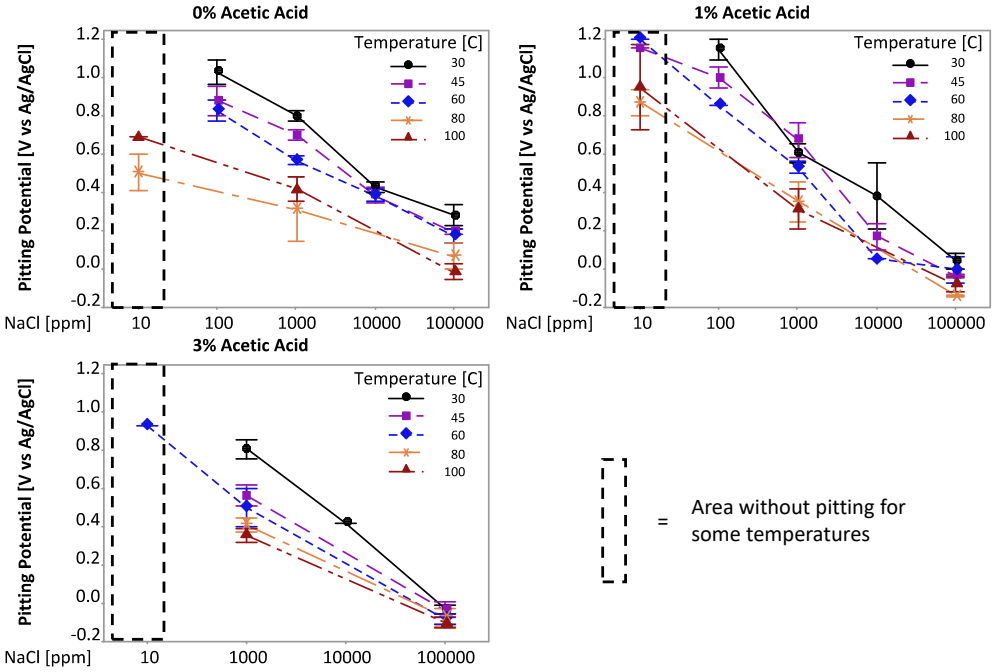

Figure 15: Effect of temperatures on pitting potentials at different chloride concentrations and different acetic acid concentrations. The dotted square marks an area where no pitting was initiated for some temperatures.

yet understood and the result presented in this thesis does not make the analysis easier.

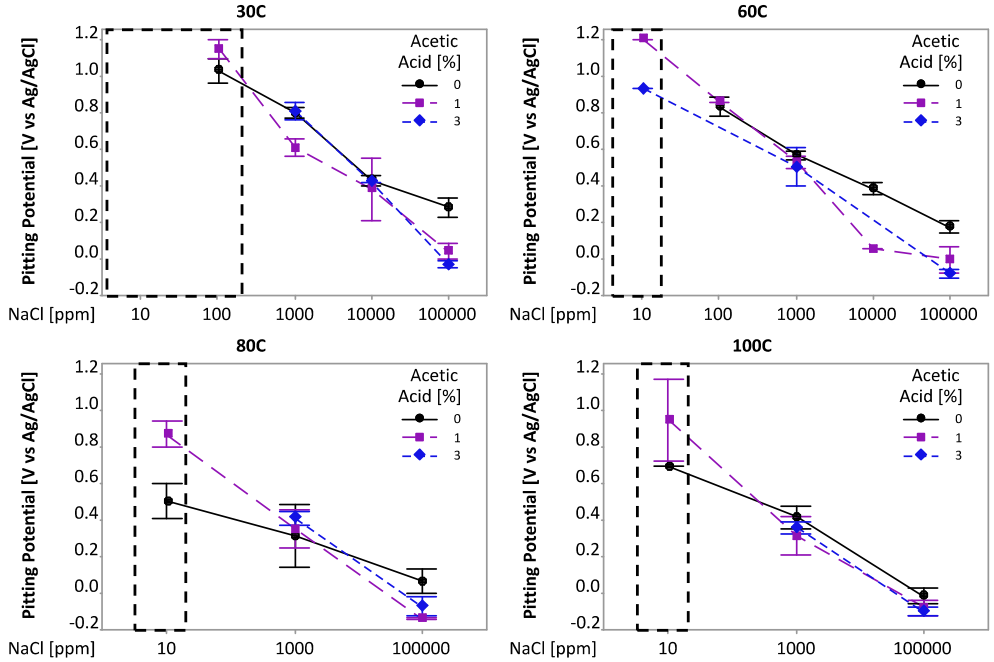

Figure 16: Effects of acetic acid concentrations on pitting potentials plotted at different temperatures as a function of chloride concentration. The dotted square represents an area where there was an absence of pitting initiation for certain environments.

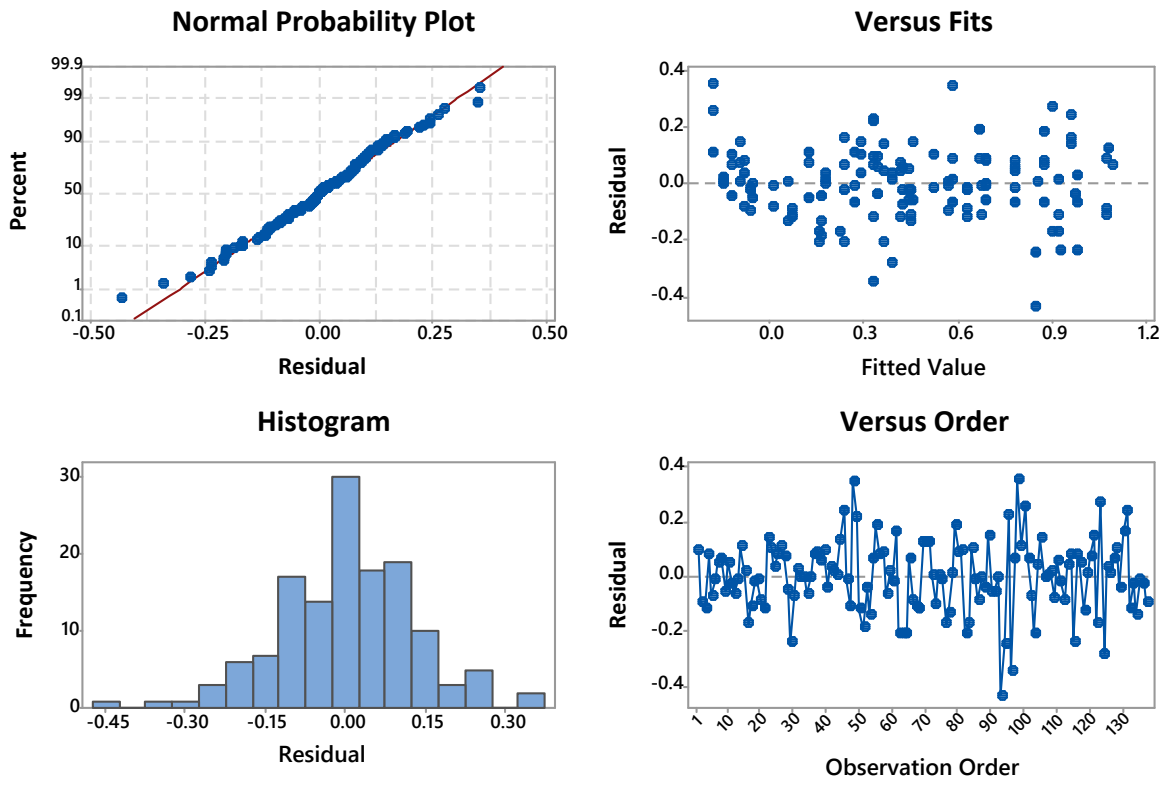

Figure 17: Residual analysis of the DOE factorial design model where crevice and transpassive behaviour has been excluded.

5.2.1 Main Effects Plots

To analyze which factors have the largest impact on pitting potential, the design of the experiment (DOE) function in Minitab was used. A DOE, in its simplest forms, creates an optimal experimental plan with different factors that could affect the experimental result in order to decrease the number of experiments required. The DOE function automatically creates an analysis of variance (ANOVA) which tries to fit a linear model for the different parameters, as well as creating a covariance analysis to examine if a covariance between factors exists [35]. An analysis of the raw residuals in the model is presented in figure 17. The normal probability plot fits quite well with some deviations towards the ends, and the histogram largely follows a normal distribution, although not ideal. In the "versus fits" graph, the residuals are plotted against the fitted value of the model. Here a random distribution is expected with an equal amount of dots above and below the line at 0. It seems to follow the expected behaviour, except for some small deviations at the extremes. One could argue there is some form of pattern and therefore bias in the model. Plotting the residuals versus order follows the same pattern as before, it appears to be a random distribution of the residuals and thus the model should fit quite well, albeit it is not perfect. The R^2 value for the model is 0.8843 but the purpose of this analysis is not to predict values in the future, only to examine the main effects and the correlation between factors. Thus, a high R^2 value is not necessary. The regression equation for pitting potential can be found in appendix A.2.

A factorial analysis was done for temperature, acetic acid and chloride concentration. The result is presented as the main effects plot shown in figure 18. The main effect indicates which factors have the strongest impact on the pitting potential, a steeper gradient means a stronger correlation. The NaCl concentration clearly has the strongest impact on pitting potential on all levels from 10 - 100 000 ppm. The temperature has the second strongest interaction, it also seems like the pitting potential is not affected between 80 and 100 °C. Acetic acid seems to have a small effect on the pitting potential between 0% and 1% but no difference between 1% and 3%. The effects from temperature (P=0), chloride (P=0) and acetic acid (P= 0.037) were statistically significant, at $\alpha = 0.05$. It was not possible to model any covariance between the parameters. Therefore, it can be concluded that the factors do not affect each other in any significant way. Raw data from the ANOVA can be found in appendix A.2.

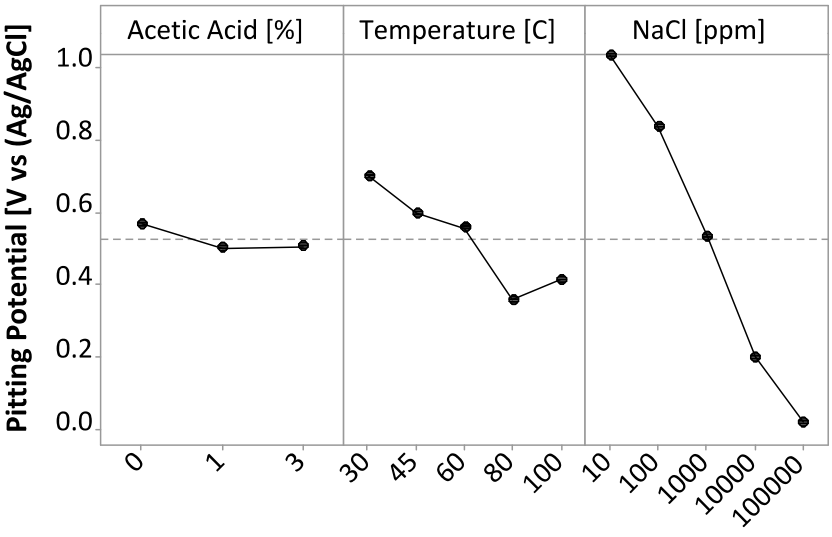

Figure 18: The main effects plotted for acetic acid, Temperature and chloride concentration where crevice and transpassive behaviour has been excluded. A steeper curve represents a larger effect, a horizontal curve indicates no effect.

5.2.2 Deviating Experiments

Nine measurements deviated largely from the rest, 1 at 30 °C, 4 at 80 °C and 4 at 100 °C. This suggests there are larger deviations at higher temperatures, a reasonable result. Higher temperature affects the properties of the test setup, for example, the O-ring becomes softer and may change its morphology. Higher temperatures also lead to larger fluctuations in temperature since the heating unit operates on a simple P-regulator. When the temperature is below the set point, it starts the heating unit and when a temperature above the set point is reached, the heating unit is switched off. When running tests at 80 or 100 °C, the fluctuations become much larger. Furthermore, it takes time to heat the solution to the proper temperature. It took about 10 minutes more to heat the solution to 100 °compared to 30 °C, therefore the sample spent more time in contact with the solution at high temperatures before the measurements began. These are all factors that may explain the larger error margins at higher temperatures.

5.2.3 Engineering Diagrams

Engineering diagrams were designed based on the pitting potentials to map areas where pitting was present vs where the metal was stable, as shown in figure 19 and 20 . Solid squares, ■, indicate a lower pitting potential than the selected one (meaning pitting corrosion occurred) and open squares, □, indicate an equal or higher pitting potential. Figure 20 is an enlarged version of figure 19e (500 mV, 1% acetic acid) but has a line drawn to further clarify where pitting occurs. Above the line, pits formed and below the line, the sample was stable. There are different amounts of data points in the graphs since measurements at 80 °C, 100 °C and 3% acetic acid were only done at three different chloride concentrations. It shows that temperature dependence is most prominent at medium chloride concentrations (1000 ppm), and for higher chloride concentrations there is mainly chloride dependence (and temperature independence). At low chloride concentrations and 0% acetic acid (figure 19g and 19j) there is a temperature dependence while no temperature dependence was seen when acetic acid was added. A small deviation can be seen in figure 19g where there is pitting at 10 ppm, 80 °C but not for 10 ppm, 100 °C. This deviation may be caused by the uncertainties seen at high temperatures described earlier. This engineering diagram is very useful for analysing and comparing different polarization experiments, but it is difficult to translate these results to assess corrosion risk in physical reality.

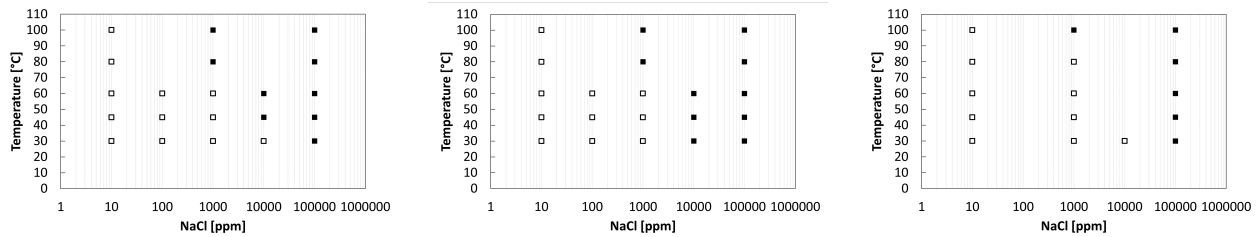

(a) 400 mV (Ag/AgCl) 0% HAc (b) 400 mV (Ag/AgCl) 1% HAc (c) 400 mV (Ag/AgCl) 3% HAc

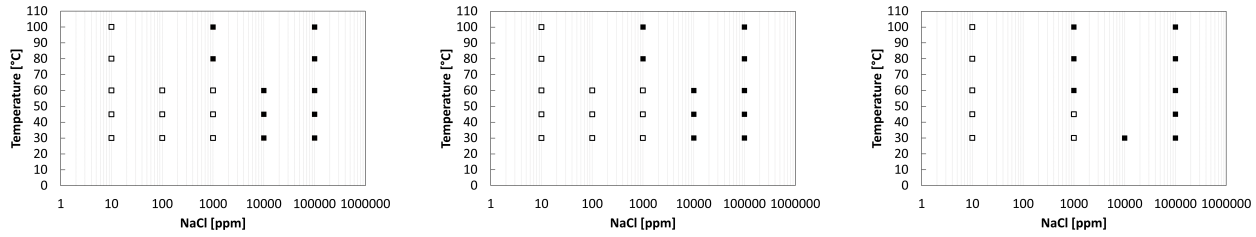

(d) 500 mV (Ag/AgCl) 0% HAc (e) 500 mV (Ag/AgCl) 1% HAc (f) 500 mV (Ag/AgCl) 3% HAc

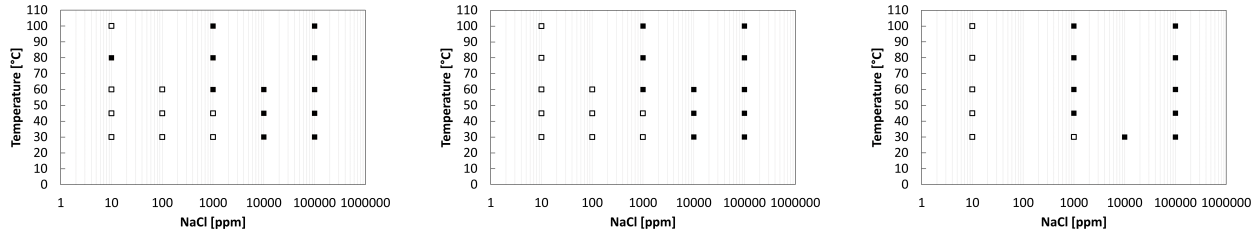

(g) 600 mV (Ag/AgCl) 0% HAc (h) 600 mV (Ag/AgCl) 1% HAc (i) 600 mV (Ag/AgCl) 3% HAc

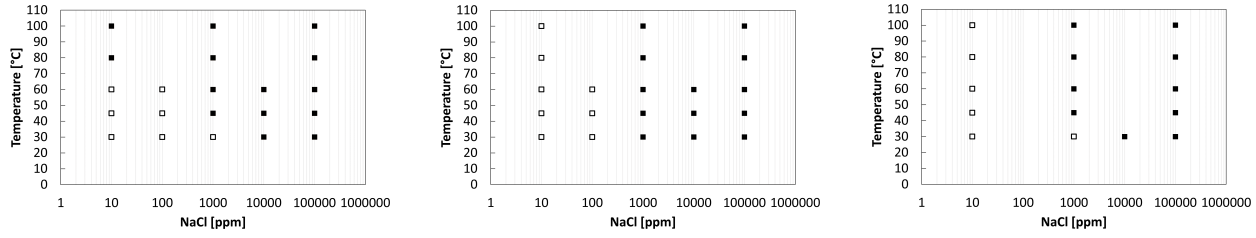

(j) 700 mV (Ag/AgCl) 0% HAc (k) 700 mV (Ag/AgCl) 1% HAc (l) 700 mV (Ag/AgCl) 3% HAc

Figure 19: Potential diagram at different selected potentials and acetic acid concentrations. Solid squares, ■, indicate a lower pitting potential than the selected one and open squares, □, indicate an equal or higher pitting potential.

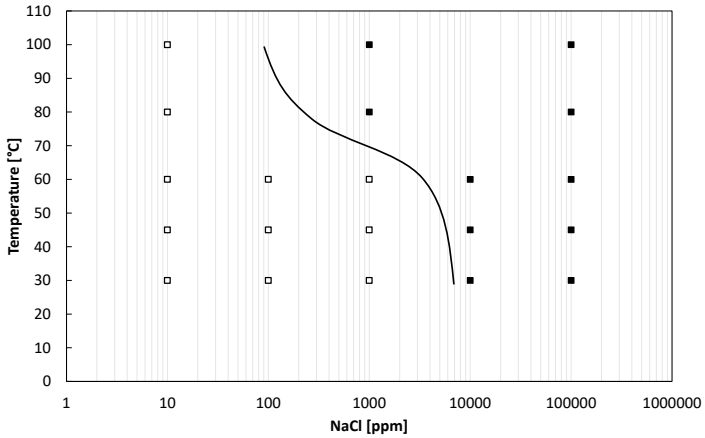

Figure 20: Engineering diagram with a line where above the line, pitting occurs and below the metal is stable.

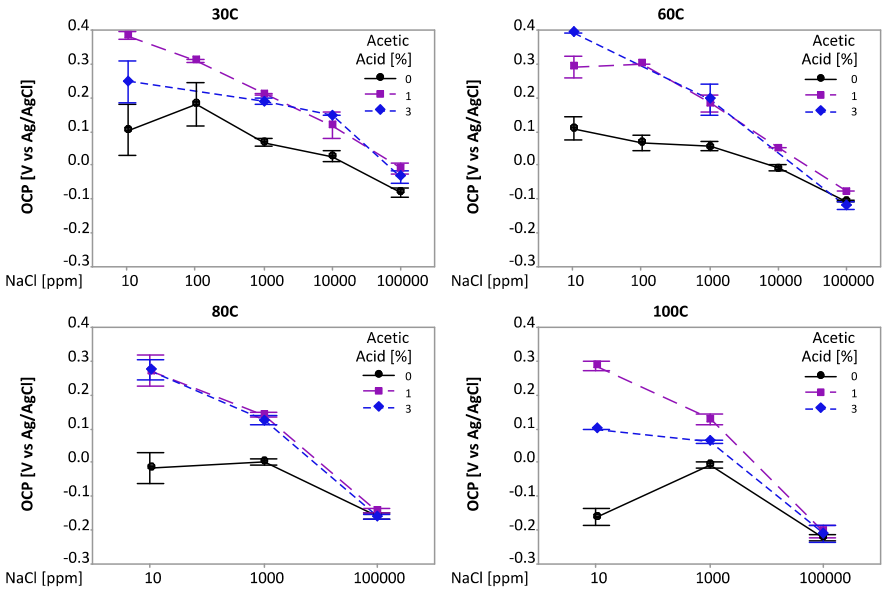

Figure 21: Summary of average OCP measurements at different temperatures for the three levels of acetic acid concentration.

5.3 OCP Measurements

The OCP measurements are plotted in figure 21. A higher chloride concentration decreases the OCP value, adding acetic acid increases the OCP value and increasing the temperature decreases the OCP value. As discussed earlier in section 2.6.2, a higher OCP value indicates a stronger corrosion resistance, therefore it is reasonable that increasing chloride concentration and raising the temperature decrease the OCP value since the metal is more prone to corrode. These result also correlates with the pitting potential data. The effect of acetic acid on the OCP value, which shows a strong correlation, indicates acetic acid should increase the pitting potential since the OCP values are increased, This effect does correlate for pitting measurements at low chloride concentrations, but not for any concentrations above 10 ppm. Perhaps this difference is because of the difference in measurement techniques. The reaction that takes place at the corrosion potential (OCP) may differ a bit from the reaction at polarization measurements since a potential is applied. The protective characteristics of acetic acid may be more prominent in neutral environments compared to when voltages are applied. For 30, 80 and 100 °C there is a drop in OCP value for 10 ppm compared to all other chloride concentrations, the reason for this is not understood.

5.4 Perssons Acetic Acid Compared to Pure Acetic Acid

Perstorp's 24% acetic acid was used for all experiments because it resembles what is commonly used in the food industry, ketchup, for example, uses acetic acid at a concentration of about 1% and chemically pure acetic acid is not used. To determine that Perstorps acetic acid doesn't have any additives that affect the results, experiments at the same concentration of acetic acid were done with Perstorp and chemically pure (99.9%) acetic acid. The result, provided in figure 22, shows no notable difference between chemically pure and food-grade acetic acid.

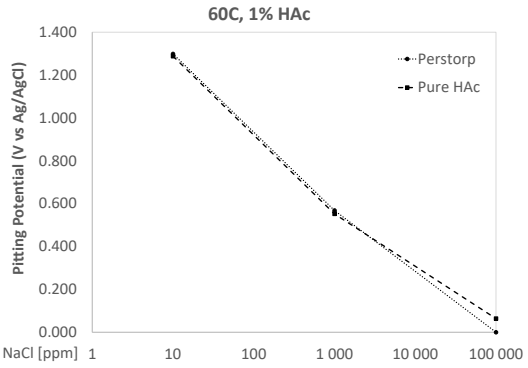

Figure 22: Experiments comparing Perstorp's 24% acetic acid with chemically pure acetic acid at different chloride concentrations.

5.5 Neural Network Image Analysis

In earlier sections, analysis by electrochemical means have been used, and they are a good to analyse when pitting corrosion occurs, but it does not say anything about the mor-

phology of the pits. It could be interesting to understand the area of a pit, or how many pits there are, maybe also how the deposition of corrosion product changes with environment. Therefore, a method to automatically detect corrosion on the samples was developed by Andrii Hrechuk, postdoc at Lund University, using neural networks. Specifically, a convolutional neural network called the U-net was used in order to automatically detect the corrosion. This type of network can be trained to localize certain features with high precision using relatively small numbers of data [36]. To begin with, the samples were photographed by a camera where the light source shifted direction around the sample and an image was taken for each separate direction. Thereafter, the original images was masked in three different regions by hand; Background, sample, and corrosion spot. This can be seen in figure 23 where (a) is the original image, (b) shows the three different regions marked manually where the dark grey is the background, black is the sample and the light gray curved line is the corrosion spot. By manually marking these areas, the U-net is trained to automatically localize these areas, as can be seen in (c) where it shows the background as blue, the sample as no colour, and the corrosion area with a yellow mark. The technique shows promising results, and experiments to mark more areas are being investigated. For example, localizing corrosion deposits on the surface is another parameter that could be interesting. When the deep learning is finished, the idea is to put the sample in a holder, let it be photographed, and receive values for number of pits, the area of each pit, and how much corrosion product has deposited.

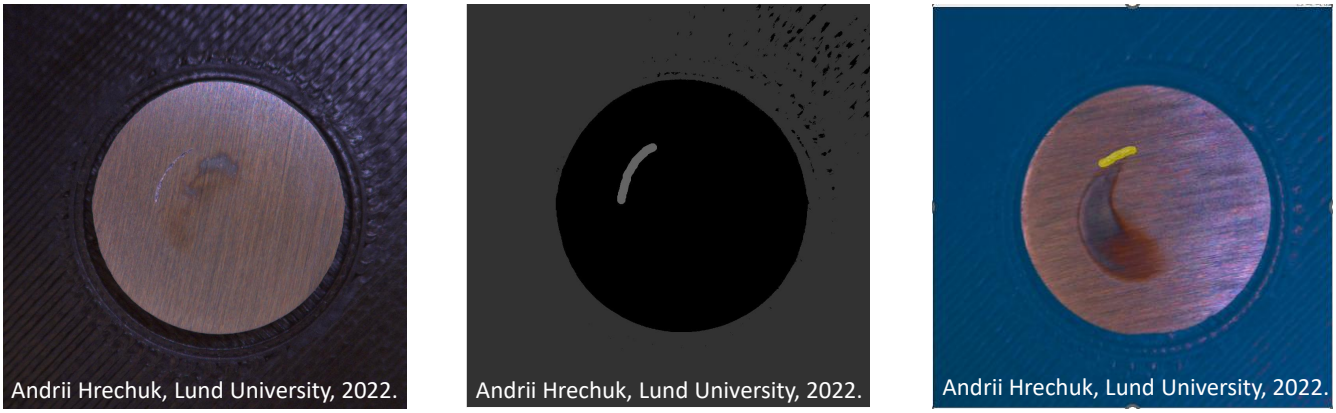

Figure 23: Principle of the deep learning to localize three different areas, background, sample and corrosion spots.

6 Conclusion

1. The newly developed test holder for electrochemical measurements inside a pasteurizing machine shows promising results but can be further developed to decrease the risk of crevice corrosion. Being able to do potentiodynamic corrosion measurements inside a pasteurizing machine opens up possibilities for a vast number of environments which previously have not been analysed.

2. Chloride ions have the largest effect on pitting potential followed by temperature. An increase in temperature decreases the pitting potential up to 80 °C, but an increase to 100 °C does not seem to further decrease the pitting potential. The relatively small standard deviations make it possible to create pitting engineering diagrams to evaluate areas where pitting occurs or not. It is, however, difficult to translate these results into physical reality.

3. Acetic acid has some effect on the pitting potentials. At low chloride concentrations (10 ppm), acetic acid increases the pitting potential but this effect is not seen at higher chloride concentrations. Increasing the concentration from 1% to 3% does not affect the pitting corrosion in any significant way.

4. Low chloride concentrations (10 ppm) were generally difficult to analyze,

5. There is no difference between food-grade acetic acid (Perstorp's 24%) compared to chemically pure acetic acid (99.9%) when diluted to the same concentration.

6. Increasing chloride concentration and temperature decrease the OCP, indicating a lower corrosion resistance while acetic acid increases the OCP. An increase in OCP indicates higher corrosion resistance, however, potentiodynamic measurements could not find such a correlation.

7 Outlook

There are many possible and exciting parameters to explore in the future.

- Further development of test holder to make it both more robust and decrease the possibility of crevice corrosion. A suggestion for new holder design was presented earlier in this report in section 3.1. Another possible way is to try and mimic the Avesta cell, however, it is not trivial to create a good back-pressure with the de-ionized water.

- How does bending/deforming of metal affect corrosion? This could be done by using a puncher with a small extrusion from it, causing a dent in the middle of the sample. Residual stress, such as bending, strongly affects the microstructure of the metal, as well as an increase in the number of dislocations, all parameters known to affect corrosion resistance [37, 38].

- How do proteins affect corrosion? Since a pasteurizing machine is used, which heats and cools the solution inside repeatedly, it is possible to use solutions such as milk. In an ordinary setup, the proteins would denature due to the high temperatures. Here lies an exciting possibility to evaluate how, for example, milk proteins affect localized corrosion.

- Different types of steel grades.

- Analyse how different flow rates inside the pasteurizer affect the pitting potentials. A higher flow probably leads to an increase in pitting potential.

- Further research within image and neural network analysis of how the corrosion morphology is affected by different parameters. It has, for example, been reported that adding acetic acid to the solution creates larger pits, but at fewer sites, [33].

- Surface roughness effect on corrosion. Could be done in different ways, grinding with finer and finer grit paper. A comparison between different grinding patterns could also be done where one sample is ground with all crevices in one direction, and the other sample is ground "randomly".

References

[1] I. Olefjord and L. Wegrelius, "Surface analysis of passive state," *Corrosion Science*, vol. 31, pp. 89–98, 1990, passivation of metals and semiconductors. [Online]. Available: https://www.sciencedirect.com/science/article/pii/0010938X9090095M

[2] S. Mameng, R. Pettersson, and J. Jonson, "Limiting conditions for pitting corrosion of stainless steel en 1.4404 (316l) in terms of temperature, potential and chloride concentration," *Materials and Corrosion*, vol. 68, no. 3, pp. 272–283, 2017.

[3] D. Han, Y. Jiang, C. Shi, B. Deng, and J. Li, "Effect of temperature, chloride ion and ph on the crevice corrosion behavior of saf 2205 duplex stainless steel in chloride solutions," *Journal of materials science*, vol. 47, no. 2, pp. 1018–1025, 2012.

[4] E. Abd El Meguid, V. Gouda, and N. Mahmoud, "Pitting corrosion behaviour of type sus904l and sus316l stainlesssteels in chloride solutions," *Materials transactions-JIM*, vol. 35, no. 10, pp. 699–702, 1994.

[5] J. Davis and A. Committee, *Stainless Steels*, ser. ASM specialty handbook. ASM International, 1994. [Online]. Available: https://books.google.se/books?id=OrlG98AHdoAC

[6] Outokumpu, "Supra 316l/4404," Retrieved 2022-10-26. [Online]. Available: https://secure.outokumpu.com/steelfinder/properties/GradeDetail.aspx?OTKBrandNameID=00602&Category=Supra

[7] E. McCafferty, *Introcudction to Corrosion Science*. Springer, 2010.

[8] G. Tranchida, M. Clesi, F. Di Franco, F. Di Quarto, and M. Santamaria, "Electronic properties and corrosion resistance of passive films on austenitic and duplex stainless steels," *Electrochimica Acta*, vol. 273, pp. 412–423, 2018. [Online]. Available: https://www.sciencedirect.com/science/article/pii/S0013468618307977

[9] V. Maurice, H. Peng, L. H. Klein, A. Seyeux, S. Zanna, and P. Marcus, "Effects of molybdenum on the composition and nanoscale morphology of passivated austenitic stainless steel surfaces," *Faraday discussions*, vol. 180, pp. 151–170, 2015.

[10] R. François, S. Laurens, and F. Deby, "1 - steel corrosion in reinforced concrete," in *Corrosion and its Consequences for Reinforced Concrete Structures*, R. François, S. Laurens, and F. Deby, Eds. Elsevier, 2018, pp. 1–41. [Online]. Available: https://www.sciencedirect.com/science/article/pii/B9781785482342500019

[11] M. Quraishi, J. Rawat, and M. Ajmal, "Macrocyclic compounds as corrosion inhibitors," *Corrosion*, vol. 54, no. 12, 1998.

[12] B. Zhang, J. Wang, B. Wu, X. Guo, Y. Wang, D. Chen, Y. Zhang, K. Du, E. Oguzie, and X. Ma, "Unmasking chloride attack on the passive film of metals," *Nature communications*, vol. 9, no. 1, pp. 1–9, 2018.

[13] H.-H. Strehblow and P. Marcus, "Mechanisms of pitting corrosion," *Corrosion mechanisms in theory and practice*, vol. 201, p. 238, 1995.

[14] F. A. Cotton, G. Wilkinson, C. A. Murillo, and M. Bochmann, *Advanced inorganic chemistry*. John Wiley and Sons, Inc., 1999.

[15] T. Hoar, "The breakdown and repair of oxide films on iron," *Transactions of the Faraday Society*, vol. 45, pp. 683–693, 1949.

[16] N. Sato, "A theory for breakdown of anodic oxide films on metals," *Electrochimica Acta*, vol. 16, no. 10, pp. 1683–1692, 1971. [Online]. Available: https://www.sciencedirect.com/science/article/pii/001346867185079X

[17] S. Gao, C. Dong, H. Luo, K. Xiao, and X. Li, "Electrochemical behavior and nonlinear mott-schottky characterization of a stainless steel passive film," *Analytical Letters*, vol. 47, no. 7, pp. 1162–1181, 2014.

[18] N. Hara, K. Hirabayashi, Y. Sugawara, and I. Muto, "Improvement of pitting corrosion resistance of type 316l stainless steel by potentiostatic removal of surface mns inclusions," *International Journal of Corrosion*, vol. 2012, 2012.

[19] M. Greene and Fontana, *Corrosion Engineering*, 3rd ed. Springer, 2010.

[20] G. Sander, V. Cruz, N. Bhat, and N. Birbilis, "On the in-situ characterisation of metastable pitting using 316l stainless steel as a case study," *Corrosion Science*, vol. 177, p. 109004, 2020. [Online]. Available: https://www.sciencedirect.com/science/article/pii/S0010938X20316231

[21] G. Wranglén, *Korrosionslära*. KTH, 1967.

[22] D. o. C. KTH, "Downloads," Retrieved 2022-10-31. [Online]. Available: https://www.kth.se/che/medusa/downloads-1.386254

[23] C. G. Zoski, *Handbook of electrochemistry*. Elsevier, 2006.

[24] R. W. Revie and H. H. Uhlig, *Corrosion and Corrosion Control - An Introduction to Corrosion Science and Engineering*, 4th ed. Wiler-Interscience, 2008.

[25] A. Södergård and M. Stolt, "Properties of lactic acid based polymers and their correlation with composition," *Progress in Polymer Science*, vol. 27, no. 6, pp. 1123–1163, 2002. [Online]. Available: https://www.sciencedirect.com/science/article/pii/S0079670002000126

[26] Ensinger, "Tecapeek mt natural," Retrieved 2022-11-14. [Online]. Available: https://www.ensingerplastics.com/sv-se/halvfabrikat/produkter/medicin-peek-tecapeek-mt-natural#/product-technical-detail-collapse-item-3-lvl-1

[27] BioLogic, "Avesta cell," Retrieved 2022-11-14. [Online]. Available: https://www.biologic.net/accessory/avesta-cell/

[28] S. S. Institute, "Svensk standard ss-iso 15158:2014," *SIS*, vol. 1, 2014.

[29] G. Instruments, "Convert potentials to another reference electrode," Retrieved 2022-11-07. [Online]. Available: https://www.gamry.com/resources-2/electrochemical-calculators-tools/convert-potentials-to-another-reference-electrode/

[30] D. Han, Y. Jiang, C. Shi, B. Deng, and J. Li, "Effect of temperature, chloride ion and ph on the crevice corrosion behavior of saf 2205 duplex stainless steel in chloride solutions," *Journal of materials science*, vol. 47, no. 2, pp. 1018–1025, 2012.

[31] A. Fattah-Alhosseini, A. Saatchi, M. Golozar, and K. Raeissi, "The transpassive dissolution mechanism of 316l stainless steel," *Electrochimica Acta*, vol. 54, no. 13, pp. 3645–3650, 2009.

[32] J. Park, S. Matsch, and H. Böhni, "Effects of temperature and chloride concentration on pit initiation and early pit growth of stainless steel," *Journal of the Electrochemical Society*, vol. 149, no. 2, p. B34, 2001.

[33] H. Zhang, W. Huang, H. Wei, Z. Chen, J. Cao, Y. Tang, X. Zhao, and Y. Zuo, "Effect of hac on the metastable pitting corrosion of 304 ss in nacl solution," *Materials*, vol. 15, no. 10, p. 3618, 2022.

[34] J. Amri, E. Gulbrandsen, and R. P. Nogueira, "Role of acetic acid in co2 top of the line corrosion of carbon steel," in *CORROSION 2011*. OnePetro, 2011.

[35] Minitab, "Minitab 21 support," Retrieved 2022-11-09. [Online]. Available: https://support.minitab.com/en-us/minitab/21/help-and-how-to/statistical-modeling/doe/how-to/factorial/analyze-factorial-design/perform-the-analysis/select-the-graphs-to-display/?SID=60508

[36] O. Ronneberger, P. Fischer, and T. Brox, "U-net: Convolutional networks for biomedical image segmentation," in *International Conference on Medical image computing and computer-assisted intervention*. Springer, 2015, pp. 234–241.

[37] K. Bertsch, G. M. De Bellefon, B. Kuehl, and D. Thoma, "Origin of dislocation structures in an additively manufactured austenitic stainless steel 316l," *Acta Materialia*, vol. 199, pp. 19–33, 2020.

[38] T. Voisin, R. Shi, Y. Zhu, Z. Qi, M. Wu, S. Sen-Britain, Y. Zhang, S. Qiu, Y. Wang, S. Thomas *et al.*, "Pitting corrosion in 316l stainless steel fabricated by laser powder bed fusion additive manufacturing: a review and perspective," *JOM*, pp. 1–22, 2022.

[39] B. Bennett and H. Pickering, "Effect of grain boundary structure on sensitization and corrosion of stainless steel," *Metallurgical Transactions A*, vol. 18, no. 6, pp. 1117–1124, 1991.

[40] Prosense, "Testing the viability of ag/agcl reference electrodes," Retrieved 2022-09-21. [Online]. Available: https://www.prosense.net/downloads/PS/Manuals/BASinc%20Electrodes/PSMF2052-PSMW2030-PSMW2021%20Ag-AgCl%20Reference%20electrodes.pdf

A Appendix

A.1 Further Reading

- **Manganese Inclusions as Pitting Initiator [18]**

- **Grain boundary structures affects on stainless steel corrosion [39]**

A.2 Statistical Analysis Data

Analysis of Variance

Source	DF	Adj SS	Adj MS	F-Value	P-Value
Model	10	17.5210	1.75210	86.98	0.000
Linear	10	17.5210	1.75210	86.98	0.000
Acetic Acid [%]	2	0.1358	0.06792	3.37	0.037
Temperature [C]	4	1.5763	0.39409	19.56	0.000
NaCl [ppm]	4	15.6307	3.90767	193.99	0.000
Error	126	2.5381	0.02014		
Lack-of-Fit	40	1.4514	0.03628	2.87	0.000
Pure Error	86	1.0868	0.01264		
Total	136	20.0591			

Model Summary

S	R-sq	R-sq(adj)	R-sq(pred)
0.141929	87.35%	86.34%	84.70%

Coefficients

Term	Coef	SE Coef	T-Value	P-Value	VIF
Constant	0.5243	0.0152	34.58	0.000	
Acetic Acid [%]					
0	0.0430	0.0172	2.50	0.014	1.16
1	-0.0242	0.0176	-1.37	0.172	1.15
Temperature [C]					
30	0.1745	0.0252	6.94	0.000	1.60
45	0.0734	0.0235	3.12	0.002	1.56
60	0.0316	0.0240	1.31	0.191	1.48
80	-0.1672	0.0274	-6.10	0.000	1.68
NaCl [ppm]					
10	0.5088	0.0350	14.53	0.000	3.06
100	0.3127	0.0341	9.18	0.000	2.89
1000	0.0075	0.0215	0.35	0.726	2.05
10000	-0.3241	0.0304	-10.67	0.000	2.62

Regression Equation

Pitting potential [V] = 0.5243 + 0.0430 Acetic Acid [%]_0 - 0.0242 Acetic Acid [%]_1
- 0.0188 Acetic Acid [%]_3 + 0.1745 Temperature [C]_30
+ 0.0734 Temperature [C]_45 + 0.0316 Temperature [C]_60
- 0.1672 Temperature [C]_80 - 0.1123 Temperature [C]_100
+ 0.5088 NaCl [ppm]_10 + 0.3127 NaCl [ppm]_100
+ 0.0075 NaCl [ppm]_1000 - 0.3241 NaCl [ppm]_10000
- 0.5049 NaCl [ppm]_100000

Figure 24: Data collected from the factorial model and ANOVA analysis where crevice and transpassive data are excluded.

A.3 Risk Asessment

Working with water at temperatures nearing, or exceeding, 100°C poses risks. The pasterurizer is able to keep water at higher pressures reaching potential temperatures of 140°C, thus a risk assessment is necessary which is presented in table 3.
If an accident occurs, the following procedure should be followed:

1. Save the person/persons in danger.3
2. Raise the alarm – get the attention of co-workers.
3. If safe, try to shut the machine off by pressing the “NÖDSTOPP”-button (emergency button).
4. Call 112 if necessary.
5. Contact personnel responsible for the workshop.

Table 3: Risk assessment of running the pasteurizer at high temperatures and pressures.

Hazard	Damage	Existing control measure	Harm (1-5)	Likelihood (1-5)	Further controls to reduce risk	Residual risk
Hot water leakage	Severe skin damage Eye damage	Protective barriers Pressure-relief valves Signs and barricades around machine Safety instructions	3	1	Ensure barriers are properly fasten Make sure equipment is turned off when not in use Never work alone Check that pressure relief-vales works	2
Hot steam	Severe skin damage Eye damage	Protective barriers Pressure-relief valves Signs and barricades around machine	3	2	Ensure barriers are properly fasten Make sure equipment is turned off when not in use Never work alone Check that pressure relief-vales works	3
Projectiles from equipment	Risk for high-speed projectiles, Risk from light bruising to potential skin penetration Head trauma Eye injury	Protective barriers Signs and barricades around machine	3	1	Ensure barriers are properly fasten Make sure equipment is turned off when not in use Never work alone Check that pressure relief-vales works	2
Hot surfaces	Skin damage	Protective barriers Signs and barricades around machine	1	3	Ensure barriers are properly fasten Make sure equipment is turned off when not in use Never work alone Make sure machine is cooled properly before sample change	2

Furthermore, safety instructions for how to operate the machine at high temperatures will be of use to people using it in the future. The most critical point hazardous point is the ending of a measurement where the potentially hot solution is drained from the machine and metal parts may have a temperature close to 100°C. Therefore the unloading should be done with extra care. Instruction on how to start, run and stop the machine and necessary safety precautions needed is listed as follows:
If the machine hasn't been used for a while, check that the pressure relief valves work as intended. For temperatures of 140°C, the pressure relief valves should be opened at 5.5 bar (155°C).

Starting procedure

1. Notify a person responsible for the workshop that high-temperature testing is ongoing. You are not allowed to start without someone knowing you are doing high-temperature tests.
2. Put up warning signs that high temp measurements are ongoing.
3. If needed, barricade parts of the room where no person should be during the test.
4. Make sure all connections are properly attached, there should be no leakage during normal operation.
5. Mount the safety barrier and make sure it is properly attached.
6. Do a test run before starting the heating process.
7. Continuously check for leakage as the temperature and pressure are increased.
8. If something seems wrong, immediately turn the machine off by pressing "NÖDSTOPP". Let the cooling water continue to flow – this flows even if Sören is turned off.

Running the measurements

1. Regularly check for leakage and that nothing irregular has happened.
2. If irregularities are noted, shut the machine off.

Ending the measurements

1. Turn off the heat and let the machine run for a couple of minutes with the cooling water flowing
2. When the solution is sufficiently cool, the safety barrier may be removed.
3. If the solution inside the machine is cool enough, empty it into a bucket and clean Sören as usual with cold water. This should cool everything enough so it's safe to touch and change samples
4. Carefully check if the sample holder is cold enough – if high temperatures were used the holder may still be warm. In that case, let the cleaning water run through the machine for a couple of minutes.

If the machine was turned off
When the machine is turned off, the circulation of the hot solution stops. The cooling water only cools locally so large portions of the machine will still be hot.

A.4 In-depth Instructions For Sören

CE = Counter electrode, WE = Working electrode, RE = Reference electrode. An image with some compartments important for experiments is provided in figure 25.

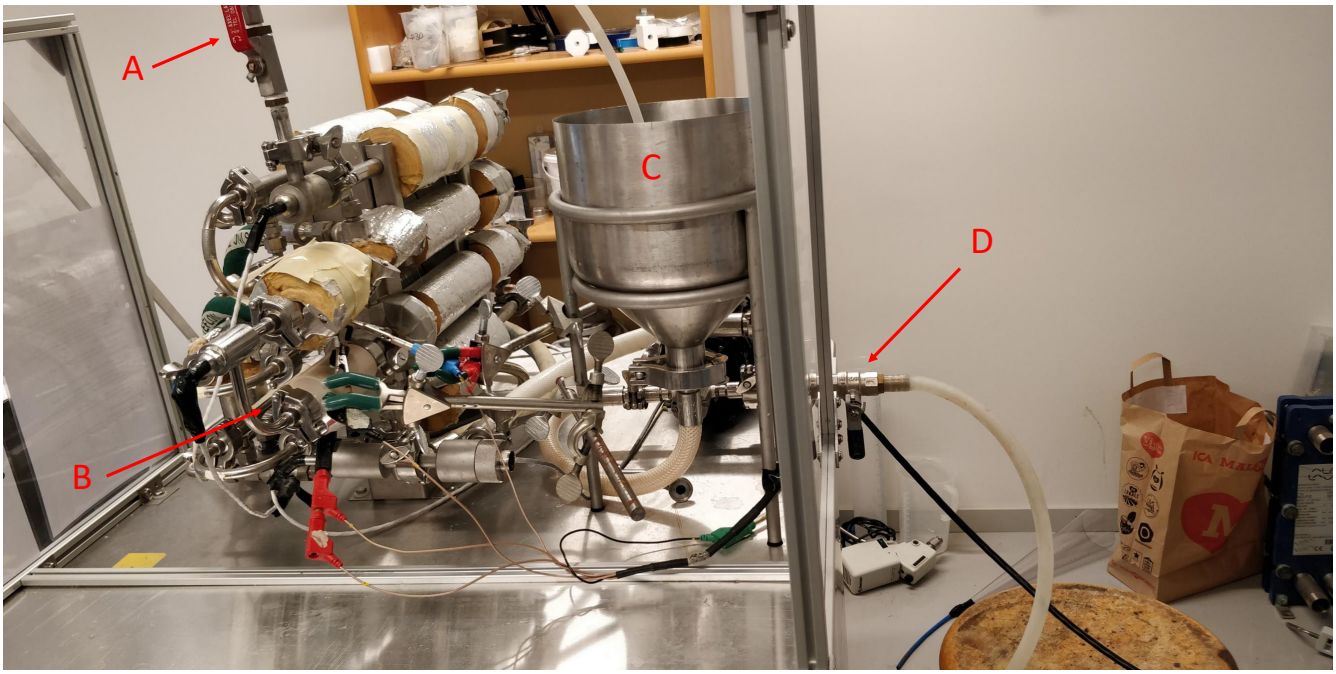

Figure 25: Sören and different compartments are shown. A is a valve to control the pressure, B is where the test holder is inserted, C is the feed tank where the solution is poured and D is a valve used to empty the solution when the experiment is finished.

A.4.1 Sample Preparation

Using the Puncher
The puncher has a specially designed 15 mm diameter stift which has a tighter fit than usual in order to decrease the deviations in sample size. When punching samples from a metal sheet, the best results are achieved by flipping the metal sheet in between each "punch" since it decreases the deformation/bending of the samples.

Grinding Samples
When handling the samples, always use plastic gloves.

1. Put the sample with the backside facing upwards and attach a strip of tape (weaving tape works really well) to the backside, see image 26.
2. Grinding should be done in three steps, 220 SiC, 500 SiC followed by 1200 Piano. A 1200-piano grinding plate designated for the corrosion tests can be found in Filip's cabinet.
3. Using the tape to keep the sample in place, apply some force in the middle of the sample. The sample should be placed somewhere between the middle and the edge of the grinding paper to make the grinding marks as straight as possible without curvature.
4. The first grinding with 220 SiC after the puncher takes some time, up to 2 minutes. Make sure that the entire surface is evenly ground without any facets before moving on to the next step.

5. Rinse the samples with water and apply soap water to remove any residue particles after each grinding step. Blow dry with air.
6. After the final grinding step (1200 piano), be extremely careful not to touch the ground surface with your fingers since this effectively ruins the samples due to the oils/fats on our fingers.
7. Store the samples in a fibre cloth and mark the grinding date.

An image with sample and weaving tape and the hand-held technique for grinding is found in figure 26.

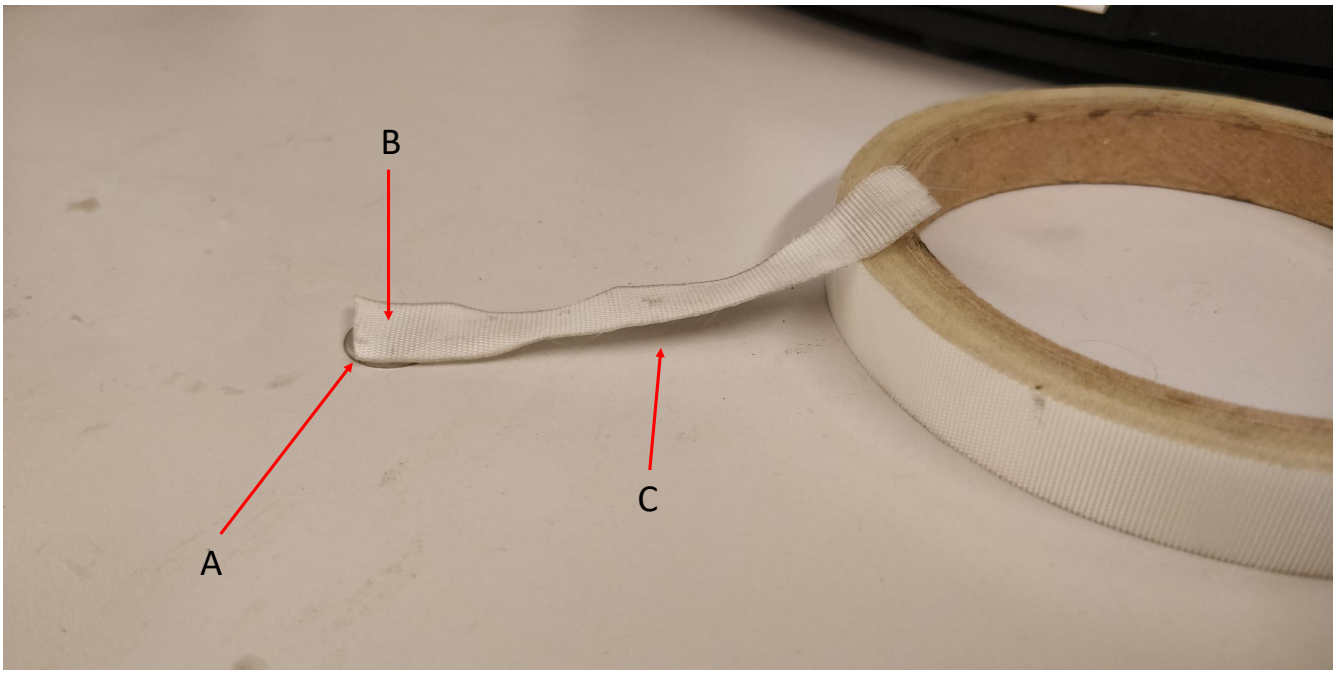

Figure 26: The method for grinding the samples using weaving tape. A is the sample facing down, B shows where you should apply force with your finger, and C shows the "handle" to keep the sample in place while you push down on the sample.

A.4.2 Test Preparation

Always use plastic gloves when handling samples.

1. Rinse samples with distilled water, followed by ethanol (or similar solution) and blow-drying with air. Double-check the samples and look for any deviations in the grinding, a small deviation to the surface may ruin the experiment since corrosion generally starts at weak points on the surface.
2. The RE (grey/beige rod) should be placed directly opposite to the metal sample and inserted a bit into the hole of the metal sample so it is only a couple of mm away from the metal surface. It should not touch the surface! Insert the CE (the black glassy carbon rod) as far as possible in the test holder without touching the inner walls. Be careful - it is expensive and brittle and easily breaks. If you are uncertain about the placement, look at figure 8 for an image of the setup.
3. The O-ring needs to be placed inside the "O-ring holder" - make sure to use a clean O-ring. The fit is pretty tight and might require some work with a tweezer. The easiest way to get it into place is to put the O-ring dead centre, drop a dummy sample on top, apply pressure to the dummy sample with a tweezer, remove the dummy sample, and use the tweezer to force the O-ring in place.

4. Put the sample on top of the O-ring with the polished side facing down towards the O-ring. Apply the metal screw, a wrench could be used to fit it tightly. Don't use too much force since this could deform the sample.

5. Attach the sample holder to Sören and make sure it is aligned in the correct direction. Attach the Nova Autolab electrodes to the WE, CE and RE (they are marked). Figure 8 shows the direction of the test holder and the connections to Nova Autolab.

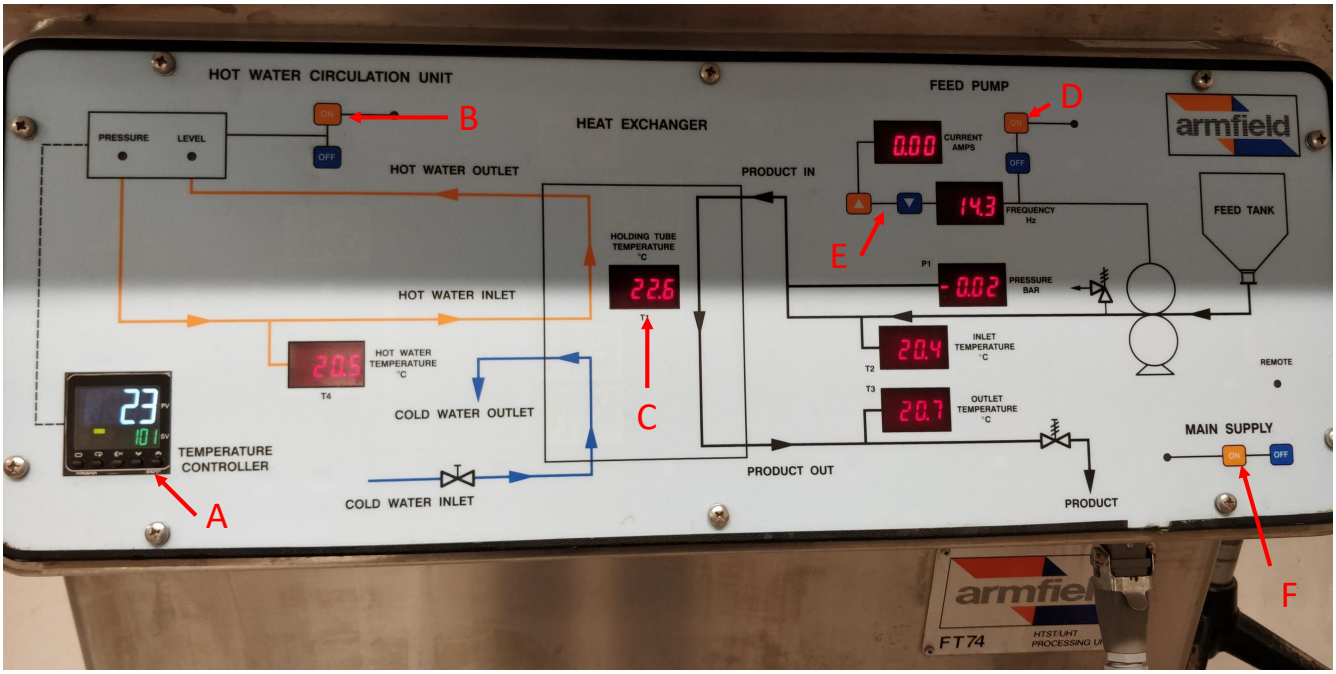

Figure 27: Image of the control panel for Sören.

A.4.3 Starting the Test

Figure 27 shows an overview of Sören's control panel. A is the set temperature for the test run. B turns on the heating unit. C shows the temperature at the test holder. E changes the pump frequency and D turns the pump on/off. F turns on the main supply to Sören. Sören has to be connected to a 32 A outlet.

1. The sample holder must be inserted before the test solution can be added, otherwise, the solution will spill out.

2. Make sure the emptying valve is closed before adding the test solution (figure 25 D).

3. A minimum of 1 L test solution is required to run the experiments.

4. Input the test parameters in Sören for the experiment. Temperature and flow rate are controlled on the Sören control panel shown in figure 27. The cooling water is controlled by a valve underneath the sink.

5. Configure the measurement in the Nova Autolab software as you want, the user manual is easy to read if you want to make changes in the test setup. If you choose to run the "Linear Polarization Standard" - a procedure designed to follow the Swedish ISO standard, the test will begin with 30 minutes of OCP followed by linear polarization starting at the OCP value. The scan rate is 0.166 mV/s, and the measurement will end at either 1.5 V or when the current exceeds 500 $\mu A/cm^2$ (which is adjusted for the small exposed surface area, so the actual current in the programme is something like 200 μA).

6. Start the heating system, cooling system and water flow in Sören and wait for the correct temperature to be reached before starting the actual measurement in Nova Autolab. You may regulate the cooling water depending on how much you want to cool the solution after heating.

7. Note the date and time when the test began.

A.4.4 Running Test and pH Measurement

1. After the test has started, in Nova Autolab, check that the OCP measurement is dynamically "living" and not static. Sometimes, the voltage will not fluctuate (in botched runs) and form a square-like curve. This indicates something is wrong with the test setup, the Autolab and PC must be restarted. An illustration of a normal/botched run is provided in figure 28.

2. After 30 minutes, take some solution in a 200 ml cup for pH measurement.

3. Rinse the pH electrode with tap water followed by distilled water and set the pH-metre to the correct measurement temperature (the same as the solution temperature in the 200 ml cup), which can be seen in the T_{out} value on the control panel of Sören. The solution should be continuously stirred with a magnetic stirrer during pH measurements to ensure the solution is not stagnant. Measure pH until a stable pH value is obtained.

4. At the same time as pH measurement, note the different parameters given by Sören for traceability.

   - Pump Frequency
   - Holding temperature
   - Inlet, outlet and hot water temperature
   - OCP-value
   - Date
   - pH value
   - Redox potential (if a redox-meter is available)

5. When the pH measurement is done, rinse the pH electrode and store it in the designated pH electrode buffer solution.

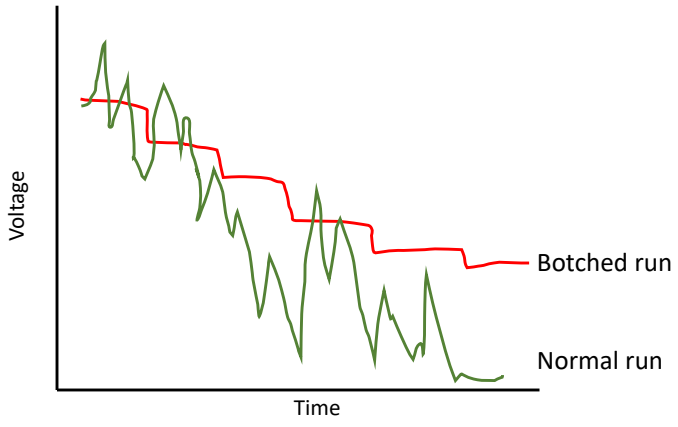

Figure 28: Illustration of a normal and botched OCP measurement.

A.4.5 Ending Measurements

In the Nova software, the continuous update symbol will stop when the measurement is finished, the graphs will also stop updating.

1. Turn off the heating and cooling water.
2. Open the "emptying" valve right next to the pump and let all water exit. You may increase the pump frequency to the max in order to speed up this process. TURN OFF the pump right BEFORE the feed tank is empty. The pump should NOT be left on while no solution is present since this may damage it.
3. Export the data from Nova Autolab software. A guide on how to export data is provided in figure 30.
4. Cleaning time!
5. Close the emptying valve and fill the feeding tank to the brim with regular water. Put the "re-feeding tube" into a separate bucket to ensure no solution is returned to the feeding tank. The re-feeding tubed is shown by the B arrow in figure 29
6. If solutions that may damage the metal were used, add more clean water into the feeding tank to properly rinse all the nasty stuff off.
7. Finally open the emptying valve to get rid of the last amount of water inside the machine.
8. Remove the test holder, unscrew the metal screw and remove the sample carefully, the easiest way is to drop it onto a fibre cloth.
9. Rinse the sample with regular water followed by distilled water.
10. Analyse the sample with an optical microscope to confirm corrosion occurred. It is a good idea to save these images for analysis in the future. A more in-depth description of the optical analysis will be provided in the next section.
11. Store the sample in some sort of container/plastic bag with the name clearly marked for re-traceability.

Figure 29: Image of the cleaning setup for Sören. The "re-feeding" tube, showcased by B should be put into a bucket so as to not reuse old water. A just points towards an ordinary bucket used as a container for the dirty water.

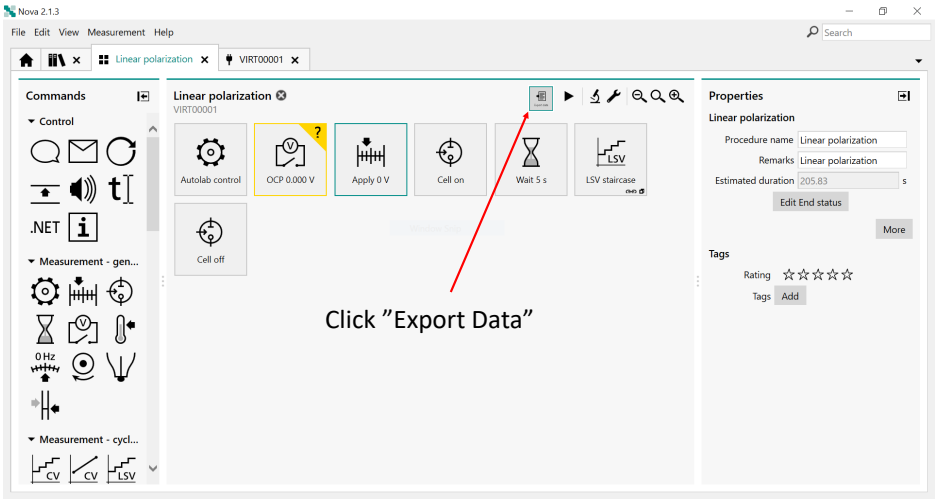

(a) When the measurement is finished, choose the graph you want to export data from and then press "Export Data" as shown in the image.

Once again, click the export data. Then choose file format/delimiter before pressing ”export”

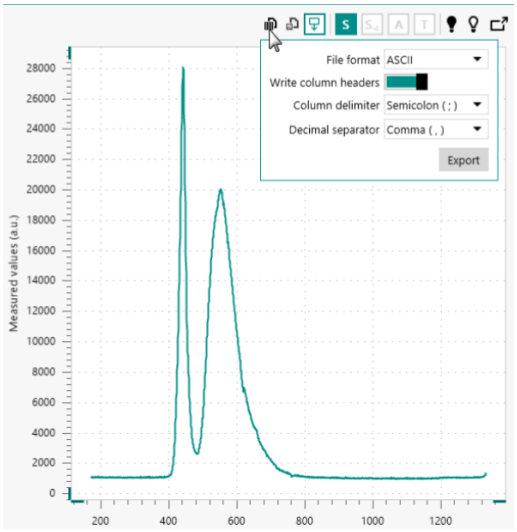

(b) When the step in (a) is completed, you once again have to press "export data", this time you get to choose the file format you will export the data as.

Figure 30

A.4.6 Optical Analysis of Samples

To confirm the formation of pits, analyze the samples in an optical microscope. It may be tricky since salt deposits may look like pits. By tilting the sample (using a tweezer) it is much easier to locate pits on the surface and rule out salt deposits since the deposits point outward from the surface. An example of a large pit with a nearby small pit is shown in figure 31, the black arrows points towards the only pits on the sample surface. The rest of the white dots are just salt deposits. Alicona may be used as a complement if uncertainties appear to further confirm pit formation, perhaps even the tabletop SEM.

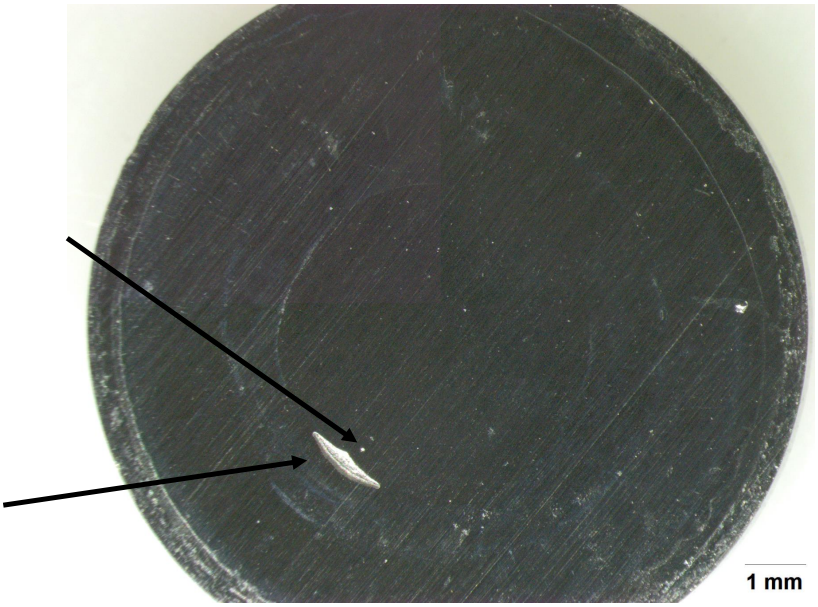

Figure 31: Optical image at 1X magnification with pits marked with black arrows

A.5 Calibration of Instruments

A.5.1 pH-electrode & ORP-electrode

Calibration of pH-electrode should be done weekly by using a three-point calibration with standardized solutions at pH 4.01, 7.00 and 10.01. These solutions are stored in the chemical cabinets in the room next to the preparation room in M-house.

A.5.2 Ag/AgCl Reference Electrode

The reference electrodes should be checked maybe every second month or after a new, high-temperature experiment has been done. Insert two RE (one used and one fabric new) into a 3M NaCl solution, both attached to a voltmeter. The potential difference between the two electrodes should not exceed 20 mV [40]. If it exceeds 20 mV, re-do the experiment a couple of times. If it still exceeds 20 mV, the used RE is probably ruined.

A.5.3 Nova Autolab PGSTAT101

Running diagnostics on the PGSTAT101 should be done somewhat regularly to check if the instrument works as intended, the PGSTAT101 comes with a built-in dummy cell for this type of diagnostic. To diagnose the internal circuits, a "Scangen" module test should be performed. A small circuit has been created for this purpose according to the user manual and is located together with other Sören parts in a cabinet in M-house. More information about the diagnostics test can be found in the Nova Autolab user manual.

A.6 Cleaning of O-ring

The O-rings required thorough cleaning to remove all precipitated NaCl from earlier experiments, if this was not removed, a locally high concentration of NaCl was created against the metal surface and the pitting potential was affected. A few cleaning methods were evaluated. Leaving them in water overnight did not clean them properly, and rinsing with ethanol and acetone did not remove more deposits than rinsing with regular water. Blow-drying the O-rings did not help either. Cleaning the O-rings by hand or with a plastic scrub was not sufficient enough. However, using a wet fibre cloth (like the ones used inside clean rooms) worked well. The wet fibre cloth was threaded through the O-ring, and then the fibre cloth was scrubbed against the O-ring while lukewarm water was continuously poured. All sides of the O-ring were scrubbed for a total time of around 30 seconds. Figure A.6 shows the O-ring directly after a test with salt deposits marked and the same O-ring after cleaning.

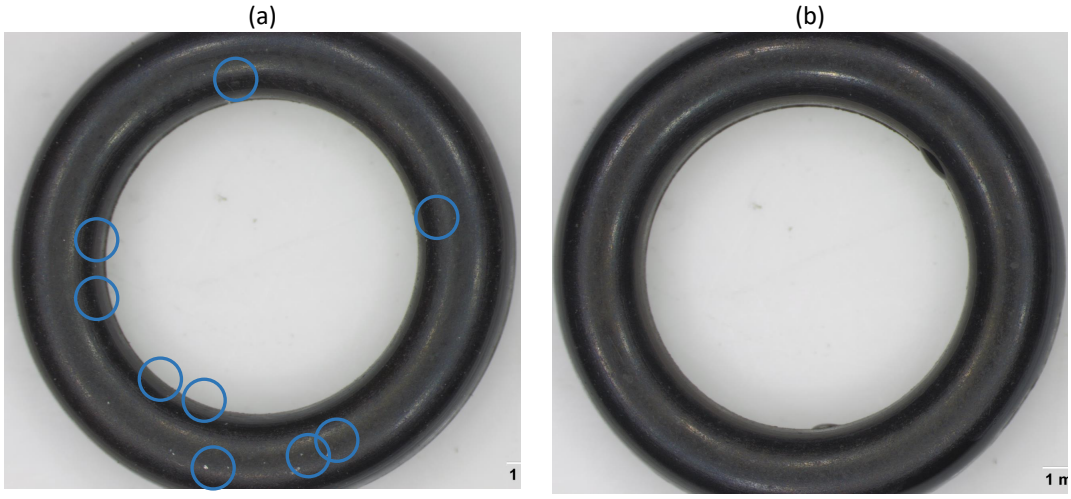

Figure 32: (a) O-ring after an experiment with salt deposits marked. (b) the same O-ring after being cleaned thoroughly with a wet fibre cloth where all salt deposits have been removed.